Spontaneous Axonal ER Ca^{2+} Waves Mediate A Shift From Action Potential-Dependent to Independent Glutamate Release in the YAC128 HD-Model

James P. Mackay[1], Caodu Buren[1], Amy I. Smith-Dijak[1], Ellen T. Koch[1], Peng Zhang, Mandi E. Schmidt[2,3], Evan Fung, Wissam B. Nassrallah[1,2], Michael R. Hayden[3], and Lynn A. Raymond[1]

[1] Department of Psychiatry, Djavad Mowafaghian Centre for Brain Health,

[2] Graduate Program in Neuroscience and MD/PhD Program,

University of British Columbia, Vancouver, British Columbia, Canada

[3] Centre for Molecular Medicine and Therapeutics, BC Children's Hospital Research Institute

Correspondence addressed to:

Lynn A. Raymond, MD, PhD

Department of Psychiatry and Djavad Mowafaghian Centre for Brain Health

University of British Columbia

4834-2255 Wesbrook Mall

Vancouver, BC Canada V6T 1Z3

Lynn.raymond@ubc.ca

Abstract

Huntington's disease (HD) is a fatal, inherited neurodegenerative disorder caused by a CAG repeat expansion in the huntingtin (HTT) gene. Altered cortical glutamate release onto striatal spiny projection neurons (SPN) is thought to contribute to pathological synaptic dysfunction in HD; however, the direction of this change is controversial and underlying mechanisms uncertain. We used the YAC128 mouse model of Huntington's disease, expressing the full-length genomic human HTT DNA with 128 repeats, to investigate this question. Here we show that in YAC128 cortical-striatal co-cultures, individual cortical terminals release vesicles onto SPNs at an increased rate compared to wild-type (WT) when action potentials (AP) are blocked with tetrodotoxin (TTX), whereas the release rate is higher in WT than YAC128 cultures when APs are intact. Further, we report increased frequency of miniature excitatory postsynaptic currents (mEPSCs) during the stage of rapid synaptogenesis *in vitro* for YAC128 cortical cultures, which can be explained by increased spontaneous Ca^{2+} released from presynaptic endoplasmic reticulum (ER) stores. Experiments in which axonal bouton Ca^{2+} was directly imaged (in TTX) with a synapsin-tagged GCaMP construct revealed higher cytosolic Ca^{2+} concentrations and more frequent axonal Ca^{2+} waves in YAC128 cultures. Conversely, in the absence of TTX, axonal boutons showed more frequent, larger amplitude Ca^{2+} events in WT cortical cultures. Releasing ER Ca^{2+} into the cytoplasm with low dose ryanodine, which we believe mimics YAC128 presynaptic Ca^{2+} conditions, reduced the amplitude of these AP-dependent Ca^{2+} events in WT but not YAC128 boutons. Low dose ryanodine similarly reduced the amplitude of cortical-evoked glutamate release in the striatum of WT, but not YAC128 mouse-derived brain slices. Together, our results demonstrate a shift toward increased spontaneous, and reduced

activity-dependent, glutamate release which may impact fidelity of excitatory transmission and synaptic plasticity.

Introduction

Huntington's disease (HD) is a fatal, autosomal dominantly-inherited neurodegenerative disorder caused by a polyglutamine-encoding CAG repeat-expansion (>35 repeats) in exon-1 of the huntingtin gene (Anon, 1993). Disease onset is typically in middle age, characterized by progressively disordered movement and declining cognition (Bachoud-Lévi et al., 2019). Although the mutant huntingtin protein (mHTT) is widely expressed, GABAergic spiny projection neurons (SPN)s of the striatum and pyramidal neurons of the cerebral cortex show the most severe degeneration in HD (Graveland et al., 1985; Vonsattel et al., 1985). Cortical glutamatergic afferents extensively innervate striatal SPNs and dysfunction at these synapses is thought to precede overt neuron loss in HD (Raymond et al., 2011).

Glutamate-mediated toxicity was initially proposed to contribute to pathogenesis in HD based on studies showing that striatal injections of glutamate receptor agonists largely recapitulate HD pathology in animals (Beal et al., 1986; Hantraye et al., 1990). More recently, studies in SPNs from transgenic and knock-in mouse models of HD demonstrate enhanced extrasynaptic N-Methyl-D-Aspartate receptor (NMDAR) surface expression and function that may explain, in part, increased susceptibility to excitotoxic challenges (Zeron et al., 2002; Fan et al., 2007; Milnerwood et al., 2010; Plotkin et al., 2014; Kovalenko et al., 2018) (Botelho et al., 2014). Cell

stress/death signaling mediated by elevated levels of extrasynaptic NMDARs in HD SPNs may be further exacerbated by reduced glutamate transporter function (Miller et al., 2008) (Cross et al., 1986; Rebec, 2018), although recent studies show glutamate clearance after synaptic release is normal or accelerated in striatal and cortical brain slice (Parsons et al., 2016). Additionally, some studies show synaptic glutamate release from cortical afferents is altered in HD mouse models, possibly contributing to excitotoxicity and synaptic dysfunction (Cepeda et al., 2003; Joshi et al., 2009; Raymond et al., 2011). However, the direction of this effect appears to be model and disease-stage dependent; relative to wildtype (WT), glutamate release is typically enhanced early, but reduced with disease progression in HD mice (Joshi et al., 2009).

Mutant HTT (mHTT) directly interacts with endoplasmic reticulum (ER) type-1 inositol (1,4,5)-triphosphate receptors (IP3R)s sensitizing their Ca^{2+} release in response to IP3 (Tang et al., 2003); blocking this interaction normalizes IP3-induced ER Ca^{2+} release *in vitro* and improves behavioral outcomes in HD-model mice (Tang et al., 2009). Furthermore, evidence suggests Ryanodine receptors, which are ER-localized Ca^{2+} channels that mediate Ca^{2+}-induced Ca^{2+} release, are constitutively leaky in HD mouse models (Suzuki et al., 2012). Although these studies focused on the soma and dendrites of SPNs at the postsynaptic side of cortical-striatal synapses, ER is found in all neuronal compartments, including presynaptic terminals, where its Ca^{2+} stores, when released, modulate neurotransmission (Llano et al., 2000; Emptage et al., 2001). However, it is unknown whether presynaptic ER Ca^{2+} handling is also dysfunctional in HD and if such a process contributes to altered glutamate release from cortical synaptic terminals.

Here, we have investigated whether glutamate release is altered, and if ER Ca^{2+} dysregulation contributes to aberrant function, in presynaptic terminals of cortical pyramidal neurons from premanifest HD-model mice expressing full-length mHTT with 128 CAG-repeats in a yeast artificial chromosome (YAC128). Our results from neuronal cultures and acute cortical-striatal brain slices demonstrate a shift in balance favoring increased action potential (AP)-independent (miniature) vs. AP-dependent glutamate release, and that altered ER Ca^{2+} release contributes to this change. Since activity-independent neurotransmission may mediate distinct physiologically relevant signaling (Kavalali, 2015), our data contribute to growing evidence for synaptic dysfunction in cortex and striatum, and support a key role for ER Ca^{2+} dysregulation in the pathophysiology of HD.

Results

Miniature glutamate release is enhanced in YAC128 cortical-striatal co-cultures at the expense of action potential-dependent release

Our group previously explored early, mutant huntingtin protein (mHTT)-mediated changes in cortical-striatal synaptic function with yeast artificial chromosome (YAC128) mouse-derived cortical and striatal neuron-containing co-cultures. At day in vitro (DIV) 14, striatal spiny projection neurons (SPN)s in these YAC128 co-cultures showed more frequent miniature excitatory postsynaptic currents (mEPSC)s (Buren et al., 2016). This genotype difference did not persist at DIV 21, at which point a reduction in YAC128 SPN total dendritic length, and

therefore reduced total excitatory synapses, may have masked an increase in presynaptic glutamate release compared to WT (Buren et al., 2016).

To more directly assess rates of presynaptic glutamate release from cortical pyramidal neurons (CPNs) onto YAC128 and WT SPNs, we incubated live co-cultures with a fluorophore-tagged antibody specific for the synaptotagmin-1 (Syt-1) protein, an important Ca^{2+}-sensor present in presynaptic vesicles (Geppert et al., 1994; Fernández-Chacón et al., 2001). Since antibody binding occurs only when exocytosis exposes the vesicle lumen to the extracellular solution, the time-dependent increase in Syt-1 stain-intensity generally reflects rates of synaptic vesicular release over the linear portion of the incubation-time vs intensity curve. Importantly, we found no genotype difference in cortical terminal Syt-1 puncta density along SPN dendrites after fixing co-cultures and immunostaining for Syt-1 (Not Illustrated).

We exogenously expressed a GFP-tagged PSD95 construct in striatal neurons to label the postsynaptic spines of SPNs and performed anti VGlut-1 immuno-staining (following live-staining with the Syt-1 extracellular-epitope antibody) to identify CPN presynaptic terminals. Syt-1 stain-intensity was measured over VGlut-1-stained puncta colocalized with the GFP-PSD95-tag. In the presence of tetrodotoxin (TTX) (500 nM), DIV21 YAC128 co-cultures showed greater Syt-1 stain-intensity than WT cultures following equivalent incubation times (Figure 1A-C). However, the opposite result was seen in the absence of TTX, specifically YAC128 cultures showed lower Syt-1 stain intensity than WT at the above glutamatergic terminals onto SPNs when action potential firing was intact (Figure 1D). These experiments

suggest enhanced miniature (mini), but reduced action potential-dependent glutamate release from YAC128 cortical terminals.

Mini EPSC frequencies are elevated in YAC128 cortical mono-cultures at early time points

To establish whether enhanced mini glutamate release is a general feature of YAC128 cortical terminals and to investigate mechanistic details of this phenomenon in a simpler preparation, we next performed experiments in WT or YAC128-derived cortical mono-cultures. We first established CPN mEPSC parameters in these cultures at various DIV ages (7, 14, 18 and 21). In general, both genotypes showed increased mEPSC frequencies with culture time. However, YAC128 CPN mEPSC frequencies were consistently higher than age-matched WT controls up until DIV 21, at which point mEPSC frequencies became comparable between genotypes **(Figure 2),** as was also the case in the co-culture model (Buren et al., 2016). The greatest genotype mEPSC frequency difference occurred at DIV 14, when mean YAC128 CPN frequencies were more than double that of WT: 10.83 ± 1.80 Hz vs 4.52 ± 0.60 Hz, respectively **(Figure 2D, E)**. YAC128 mEPSC frequencies remained significantly higher than WT at DIV18: 14.07 ± 1.54 Hz vs 9.92 ± 1.54 Hz, respectively **(Figure 2G, H)**. Age matched YAC128 and WT CPN showed similar mEPSC amplitudes across all DIV time points examined **(Figure 2 C, F, I and L)**. We chose to perform subsequent experiments probing the mechanistic details underlying increased cortical mini glutamate release in DIV 18 cortical monocultures, since this was the most mature culture stage at which mEPSC frequencies were elevated in YAC128 CPNs.

Synapse numbers and dendritic complexity are similar in WT and YAC128 cortical pyramidal neurons at DIV 18

The higher mEPSC frequencies seen in DIV 18 YAC128 CPNs suggest an increased presynaptic glutamate release probability. However, relative differences in synapse numbers could also account for this finding. To estimate numbers of synapses, we first expressed cytosolic GFP in a small proportion of neurons in WT and YAC128 cortical cultures and imaged full CPN dendritic arbors at DIV 18. Sholl analysis revealed similar arborization patterns and total dendritic length in WT and YAC128 CPNs **(Figure 3A, C)**. In separate cultures, we expressed an internal GFP-tagged anti-PSD95 antibody (Gross et al., 2013) in a subset of neurons and immuno-stained for VGlut1, to identify glutamatergic terminals, and the GLUA2 AMPA receptor subunit, to identify functional synapses. Functional synapse numbers, defined as GFP-labeled PSD95 puncta colocalized with VGlut1 and GLUA2 immunofluorescent-labeled puncta, were not significantly different between DIV 18 WT and YAC128 CPNs, with a trend towards lower synapse density in YAC128 CPNs **(Figure 3E, F)**. Together with the data in Fig. 2 showing increased mEPSC frequency in YAC128 CPNs at DIV 18 and the enhanced Syt-1 staining in TTX shown in Fig. 1, these results point to an increase in miniature vesicular glutamate release from cortical terminals in YAC128 cultures.

Releasing ER calcium with low-dose ryanodine or caffeine increases the mini EPSC frequency in WT, but not YAC128 cultures

Mouse models suggest Ca^{2+} release from ER stores is aberrant in HD due to increased IP3 and ryanodine receptor activity (Tang et al., 2003; Suzuki et al., 2012). Although effects of mHTT on the presynaptic ER have not been specifically studied, we hypothesized a presynaptic ER leak elevates cytosolic Ca^{2+}, thereby mediating the increased mini glutamate release seen in our YAC128 cultures **(Figure 4A, B)**. To test this hypothesis, we first recorded mEPSCs before and during local application of low dose (5 μM) ryanodine to cultured CPNs; 5 μM ryanodine releases ER Ca^{2+} by opening ryanodine receptors (Meissner, 2017). In WT cultures, 5 μM ryanodine nearly doubled the CPN mEPSC frequency: from 6.74 ± 1.17 Hz to 11.91 ± 2.36 Hz [Students' paired T-test; p=0.0280; n=13 cells] **(Figure 4C - E)**. In YAC128 cultures, however, ryanodine (5 μM) did not significantly alter the CPN mEPSC frequency: 11.98 ± 1.66 Hz vs 13.89 ± 2.01 Hz - under control conditions and in ryanodine (5 μM) respectively **(Figure 4F - H)**. A Comparison of the percent change in mEPSC frequency following ryanodine (5 μM) revealed a significantly greater response in WT than in YAC128 CPNs **(Figure 4I)**. We next used caffeine (1 mM) as an alternative means of agonizing ryanodine receptors; this more prominently increased the mEPSC frequency in WT cultures, but otherwise produced similar results **(Supplemental Figure 1)**.

Removing extracellular Ca^{2+} and blocking the ER SERCA pump substantially reduces the mEPSC frequency in YAC128 but not WT cultures

If an ongoing release of presynaptic ER Ca^{2+} in YAC128 cultures occludes potentiation of synaptic glutamate release by low dose ryanodine and caffeine, blocking ER Ca^{2+} release should reduce synaptic glutamate release in YAC128 cultures. To test this, we pre-incubated cultures with extracellular fluid (ECF) containing the sarco/endoplasmic reticulum Ca^{2+}-ATPase (SERCA) pump inhibitor cyclopiazonic acid (CPA) (30 μM) to deplete ER Ca^{2+} stores. Since ER Ca^{2+} depletion can increase cytosolic Ca^{2+} by engaging the store operated Ca^{2+} response, and this effect can increase mini neurotransmitter release (Emptage et al., 2001), we performed these experiments in the absence of extracellular Ca^{2+}. Under these conditions YAC128 CPNs showed a mean mEPSC frequency of 3.33 ± 0.57 Hz (n=14), significantly lower than seen in WT CPNs under identical conditions 8.41 ± 1.50 Hz (n=17) (Student's un-paired t-test; p=0.0062) **(Figure 5A, B)**. These results suggest that an ER calcium leak into the cytoplasm elevates mini vesicular glutamate release from YAC128 CPN terminals, and that in the absence of this effect, the intrinsic vesicular release probability is actually reduced in YAC128 compared to WT cortical terminals.

Spontaneous, AP-independent presynaptic Ca^{2+} sparks and waves are more frequent in YAC128 cultures

We next performed experiments using a rat synaptophysin-tagged GCaMP6-M construct (syn-GCaMP); this construct is preferentially expressed in presynaptic terminals, allowing direct

monitoring of presynaptic Ca^{2+} dynamics in our cortical culture model. This was first done in the presence of TTX (500 nM) to relate presynaptic Ca^{2+} signaling to our mEPSC findings (above). Remarkably, both YAC128 and WT cultures showed spontaneous axonal Ca^{2+} sparks, often beginning in single boutons, then initiating slow Ca^{2+} waves spreading to neighboring boutons **(Figure 6A, B)**. In some cases the above waves slowly traversed axons encompassing entire 63X (178.6 μm x 113.1 μm) imaging fields. These mini presynaptic Ca^{2+} events were strikingly slow both in decay constants, which were on average 5 - 10 times greater than typical events seen in the absence of TTX, and the rate at which these waves traversed an axon **(Figure 6A, B)**. Mini presynaptic Ca^{2+} sparks were more than three times as frequent in YAC128 cultures than in WT cultures **(Figure 6C)**, but event DF/F amplitudes did not significantly differ between genotypes **(Figure 6D)**. The detection algorithm used here (see methods) considered Ca^{2+} waves involving multiple axon boutons as single events (as in **Figure 6A**). However, the mean event area was similar in both genotypes (no illustrated), suggesting similar numbers of axonal boutons were recruited on average by such events in YAC128 and WT cultures.

Basal Cytosolic Ca^{2+} is higher in YAC128 presynaptic boutons

In a subset of TTX experiments, we applied the Ca^{2+} ionophore ionomycin (10 μM) to cultures following GCaMP imaging, which, by equilibrating the cytosol with extracellular Ca^{2+}, allows estimation of pre-ionomycin cytosolic Ca^{2+} levels. In both genotypes ionomycin-mediated changes in presynaptic GCaMP fluorescence (DF/F) were significantly smaller in boutons that had shown at least one spontaneous Ca^{2+} event in the previous 3 min recording **(Figure 7A, D)**. This suggests higher basal cytosolic Ca^{2+} concentrations in the population of synaptic boutons

that were spontaneously active in TTX. Furthermore, overall ionomycin responses were significantly smaller in YAC128 cultures than in WT cultures when comparing the entire population of boutons imaged in a culture (both spontaneously active and inactive) **(Figure 7E)**.

Caffeine increases basal Ca^{2+} and miniature events in WT, but not YAC128 cortical boutons

The slow kinetics of the above mini presynaptic Ca^{2+} events are consistent with ER-mediated Ca^{2+} waves reported in postsynaptic neuronal compartments (Ross, 2012). We next tested whether these presynaptic Ca^{2+} events were affected by Caffeine (1 mM), an ER ryanodine receptor agonist that substantially increased mEPSC frequencies in WT, but not YAC128 cultures (above). Caffeine (1 mM) significantly increased the mini presynaptic Ca^{2+} event frequency in WT cultures **(Figure 8A)**, but did not significantly alter event frequency in YAC128 cultures **(Figure 8B)**.

Significant photobleaching of the Syn-GCaMP construct occurred with prolonged imaging; this combined with the relative infrequency of mini presynaptic Ca^{2+} events necessitated imaging of separate fields for the above control and caffeine comparisons. We next performed within-bouton measurements of basal Syn-GCaMP fluorescence before and immediately following application of caffeine; the relatively short duration of these experiments made before and after measurements feasible. A clear transient slow increase in basal Syn-GCaMP fluorescence was seen in most WT boutons following caffeine (1 mM) application **(Figure 8C)**, which was generally absent or reduced in YAC128 boutons **(Figure 8D)**. Overall a significantly greater

caffeine (1 mM)-mediated increase in syn-GCaMP fluorescence was seen in WT boutons compared to YAC128 **(Figure 8E)**.

Action potential-dependent Ca^{2+} signals in presynaptic cortical terminals are less frequent in YAC128 cultures

We next used the Syn-GCaMP construct in the absence of TTX to examine presynaptic action potential-dependent Ca^{2+} signals in WT and YAC128 cortical cultures. When neuronal action potential firing was intact, Syn-GCaMP-expressing boutons in both WT and YAC128 cultures were dominated by presumably voltage gated Ca^{2+} channel-mediated signals **(Figure 9A, B)**. These signals were more frequent than those seen in the presence of TTX, but of far shorter duration. Interestingly, activity-dependent Ca^{2+} events were significantly more frequent, of a larger DF/F amplitude and of longer duration in WT cultures than in YAC128 **(Figure 9A, D).** Notably, in the absence of TTX, ryanodine (5 μM) significantly decreased the Ca^{2+} event duration in WT, but not YAC128 boutons (not illustrated). These results, together with previous experiments, suggest that releasing presynaptic ER Ca^{2+} elevates miniature vesicular glutamate release, but can also reduce activity-dependent presynaptic Ca^{2+} influx and AP-mediated glutamate release.

Low-dose ryanodine reduces evoked glutamate release in WT- but not YAC128 -derived brain slices

We next performed experiments in cortical-striatal *ex-vivo* brain slices prepared from WT and YAC128 mice expressing the fluorescent glutamate sensor iGluSnFR in striatal neurons (Parsons et al. 2016; Koch et al. 2018). This preparation allowed direct optical measurement of striatal glutamate release, independent of postsynaptic neuronal properties. Striatal iGluSnFR signals evoked by stimulating cortical axons of the corpus callosum were significantly decreased by ryanodine (5 μM) in WT, but not YAC128 slices **(Figure 10)**. These data are consistent with results in culture (Figs. 1, 9) suggesting that AP-dependent glutamate release is reduced in YAC128 as a consequence of a tonic Ca^{2+} leak from ER stores

Discussion

Presynaptic neurotransmitter release and consequent postsynaptic signaling largely underlies communication between neurons, thus forming the basis of brain circuitry. Alterations in synaptic signaling processes, particularly relating to the excitatory transmitter glutamate, have been repeatedly reported in models of HD (Raymond et al., 2011; Sepers et al., 2017; Tyebji and Hannan, 2017) and other neurogenerative diseases (Wang and Reddy, 2017). Increased cell-surface expression of extra-synaptic NMDA receptors by striatal spiny projection neurons (SPN)s favors excitotoxic postsynaptic glutamate-mediated signaling in HD-models (Milnerwood et al., 2010). Additionally, mounting evidence suggests presynaptic glutamate

release from cortical afferents is altered in HD; however, the direction of this alteration appears to be disease-stage-dependent (Cepeda et al., 2003; Joshi et al., 2009).

The endoplasmic reticulum (ER), a continuous intracellular membrane-system involved in Ca^{2+} storage and protein synthesis, is expressed in all neuronal processes including axons and presynaptic boutons. Increased cytosolic Ca^{2+}-release from the ER has been shown in HD-models, as a result of a mutant huntingtin protein (mHTT)-mediated increase in IP3 receptor responsiveness (Tang et al., 2003) and a constituent ryanodine receptor Ca^{2+} leak (Suzuki et al., 2012). Previous HD studies have focused on the postsynaptic ER, however Ca^{2+} release from the presynaptic ER is known to modulate neurotransmitter release (Llano et al., 2000; Emptage et al., 2001). Results of our study suggest mHTT expression alters ER Ca^{2+} handling at stores in close proximity to cortical presynaptic terminals, thereby altering glutamate release. This mechanism clearly increased the frequency of Ca^{2+}-dependent, action potential-independent (mini) synaptic glutamate events in our YAC128 model. Conversely, our findings suggest reduced action potential-dependent glutamate release from YAC128 cortical terminals.

Spontaneous axonal Ca^{2+} signaling increases YAC128 mini glutamate release frequencies

Glutamate, like other neurotransmitters, is released both in response to presynaptic action potential firing and spontaneously in an action potential-independent manner (mini release). Although the mechanisms governing mini release are incompletely understood, clear physiological functions of this unique form of neurotransmission have been demonstrated (McKinney et al., 1999; Frank et al., 2006; Sutton et al., 2006). Moreover, mini release can be

regulated relatively independently of its action potential-dependent counterpart and appears to be mediated by distinct vesicular pools (Sara et al., 2005; Fredj and Burrone, 2009).

In DIV 18 YAC128 cortical mono-cultures we observed more frequent mEPSCs compared to WT. Notably, no genotype differences in cortical pyramidal neuron (CPN) synapse density and dendritic morphology were evident in these cultures, indicating that mEPSC frequencies likely paralleled rates of release at individual presynaptic sites. YAC128 cortical-striatal co-cultures at DIV 21 showed higher rates of anti-synapsin-1 antibody uptake at SPN-targeting CPN boutons in TTX, revealing that individual synaptic terminals spontaneously release glutamate more rapidly. This result is consistent with a previous study indicating similar SPN mEPSC frequencies in WT and YAC128 co-cultures at DIV21 despite a reduced YAC128 SPN total dendritic length (Buren et al., 2016).

Caffeine or low dose ryanodine, which release ER Ca^{2+} by opening ryanodine receptors, failed to increase the mEPSC frequency in YAC128 CPNs, despite robustly increasing the WT mEPSC frequency. This result, in concert with the increased basal YAC128 mEPSC frequency, suggests an ongoing spontaneous Ca^{2+} store release in YAC128 cultures occludes facilitation of the mEPSC frequency by drug-mediated Ca^{2+} store release. The substantially lower CPN mEPSC frequency seen in YAC128 cultures incubated with the ER SERCA pump inhibitor CPA in 0 mM extracellular Ca^{2+}, is also consistent with a strong ER-derived Ca^{2+}-dependence of YAC128 mini glutamate release. Conversely, mEPSC frequencies in WT cultures were not substantially reduced under identical conditions; this resulted in significantly higher WT than YAC128 mEPSC frequencies in CPA and 0 mM extracellular Ca^{2+}, notably opposite the relationship seen

without CPA in standard (2 mM) extracellular Ca^{2+}. This was unexpected given overall WT and YAC128 CPN synapse numbers were similar in these cultures, but may indicate a reduction in functional YAC128 synapses, not apparent in fixed tissue images, or deficits in the YAC128 synaptic release machinery. In either case, enhanced Ca^{2+}-dependent mini glutamate release in YAC128 cultures clearly surmounts any such deficits. These results also suggest mini glutamate release in WT cultures is largely Ca^{2+}-independent. In contrast, Xu et. al (2009) reported mini glutamate release in similar cortical cultures persisted in the absence of extracellular Ca^{2+}, but was nearly completely dependent on internal Ca^{2+}stores and blocked by preincubation with the membrane-permeant Ca^{2+} chelator BAPTA-AM (Xu et al., 2009). If this were true in our cultures, we would expect Ca^{2+} store depletion (with CPA), in concert with removal of extracellular Ca^{2+}, to similarly abolish mini release. However CPA is reported to only partly deplete presynaptic ER Ca^{2+} (de Juan-Sanz et al., 2017), therefore a role of residual ER Ca^{2+} in maintaining mini release in WT cultures under these conditions cannot be excluded.

Despite a clear role of ER Ca^{2+} in mini release in a variety neuronal preparations, the temporal and spatial dynamics of action potential-independent presynaptic ER Ca^{2+} signals are largely unclear. Imaging the synapsin-GCaMP probe in TTX revealed spontaneous, presynaptic Ca^{2+} events that often initiated Ca^{2+} waves traversing cortical axons. These events were more frequent in YAC128 cultures and showed strikingly slow kinetics in both genotypes, consistent with ER Ca^{2+} waves reported in dendrites and non-neuronal cell-types (Ross, 2012). Caffeine substantially increased the mini axonal Ca^{2+} event frequency in WT cultures to levels comparable to that seen in YAC128 cultures, but failed to significantly change the event frequency in YAC128 cultures. The congruence of these results with our mEPSC findings

(above) suggests these axonal Ca^{2+} events underlie the increased YAC128 mini glutamate release frequencies.

Basal cytosolic Ca^{2+} concentrations were higher in axonal boutons showing spontaneous Ca^{2+} activity in TTX, compared to inactive boutons, in both genotypes. Elevated cytosolic Ca^{2+} levels may therefore be required to precipitate the initial ryanodine or IP3 receptor opening needed to incite the regenerative ER Ca^{2+}-induced Ca^{2+} release we presume underlie these axonal Ca^{2+} events. Interestingly, the restriction of spontaneous Ca^{2+} signals to a subset of cortical boutons with higher basal Ca^{2+} concentrations may mean mini glutamate release is not uniform across cortical boutons, but favored from this population of spontaneously active boutons. Indeed, subpopulations of synaptic boutons favoring mini release have been described in other neuronal systems (Atasoy et al., 2008; Peled et al., 2014). We suspect the higher basal cytosolic Ca^{2+} concentrations in the overall YAC128 axonal bouton population meant a greater proportion were capable of sustaining spontaneous Ca^{2+} activity. Caffeine application increased the baseline cytosolic Ca^{2+} concentration and frequency of spontaneous events in WT, but not YAC128 boutons, consistent with this idea.

Action potential-dependent glutamate release from YAC128 cortical terminals is decreased in part due to presynaptic ER depletion

The syt-1 antibody uptake assay indicated cortical terminals in YAC128 cortical-striatal co-cultures released less glutamate in response to action potential firing, compared to WT, despite increased mini release. Consistent with this, synapsin-GCaMP-expressing axonal boutons in

YAC128 cortical cultures showed fewer spontaneous Ca^{2+} events in the absence of TTX, which were of lower amplitude and of shorter average duration than those seen in WT cultures. The reduced frequency of action potential-dependent axonal Ca^{2+} events in YAC128 cultures perhaps reflects decreased CPN firing rates. However, reduced event amplitude and duration in YAC128 boutons is more consistent a reduced efficacy of action potentials at elevating cytosolic Ca^{2+}. This may be due reduced action potential-mediated discharge of the presynaptic ER, or reduced Ca^{2+} influx through voltage-gated Ca^{2+} channels.

There is a lack of consensus as to whether single action potentials can trigger Ca^{2+}-induced Ca^{2+} release from the presynaptic ER (Emptage et al., 2001), or whether prolonged, repetitive action potential firing is required (de Juan-Sanz et al., 2017). In any case, Ca^{2+}-induced Ca^{2+} release is too slow to facilitate neurotransmission associated with the inciting spike, but may play an important role in mediating release by subsequent spikes in action potential bursts. The slow kinetics of our synapsin-GCaMP probe (inherent to GCaMP constructs in general), precludes resolving the individual Ca^{2+} signals associated with bursts or otherwise closely-time action potentials. The population of longer-duration action potential-dependent synapsin-GCaMP events seen in WT, but not YAC128 cultures, may therefore reflect such burst-related signals.

Additionally, more generalized increases in cytosolic Ca^{2+} mediated by ER store release, have been shown to facilitate Ca^{2+}-dependent inactivation of voltage-gated Ca^{2+} channels including the N and P/Q-types commonly expressed in presynaptic terminals and implicated in vesicular release (Budde et al., 2002; Cens et al., 2006). If this were the case in our system, the higher

resting Ca^{2+} concentrations evident in YAC128 boutons, would be expected to leave local voltage gated Ca^{2+} channels in a higher resting state of inactivation.

Low-dose ryanodine decreased the amplitude of striatum, glutamate-mediated iGluSNR signals in WT brain slices, an effect absent or diminished in YAC128 mice, consistent with our findings in culture. It seems unlikely that the stimulation protocol used here appreciably contributed to the action potential-dependent discharged of the presynaptic ER, given the relatively low intensity stimulation used (repeated only twice at 100 Hz). Rather, we suspect a ryanodine mediated increase in presynaptic Ca^{2+} decreased evoked glutamate release by desensitizing presynaptic Ca^{2+} channels in WT slices and that this process was occlude in YAC128 slices. However, future studies will be required to clarify mechanistic details of this process.

In any effect, the totality of evidence presented here suggests enhanced spontaneous release of presynaptic ER Ca^{2+} in YAC128 mice favors mini glutamate release at the expense of evoked release.

Implications for postsynaptic signaling

Mini glutamate release elicits postsynaptic NMDA receptor-mediated Ca^{2+} influx under physiologically relevant conditions (Espinosa and Kavalali, 2009; Beaulieu-Laroche and Harnett, 2018) and can mediate postsynaptic signaling distinct from that of action potential-dependent release (Sutton et al., 2007). Indeed mini glutamate release may activate distinct populations of NMDAR receptors (Atasoy et al., 2008). Future studies will be necessary to determine if and how the increased mini glutamate release shown here interacts with the well-described

alterations in postsynaptic NMDA receptor expression in the YAC128 and other HD-models, and whether a shift towards activity-independent glutamate release plays a causal role neurodegeneration in HD.

Materials and Methods

Culture preparation:

All animal-related procedures were approved by and adhered to the guidelines of the University of British Columbia Committee on Animal Care and the Canadian Council on Animal Care (protocols A17-0295 and A15-0069). Cultures were prepared at embryonic day 17-18 from either wild-type (WT) FVB/N or transgenic, yeast artificial chromosome-containing mice expressing the full-length human huntingtin construct with 128 CAG repeats (YAC128); YAC128 mice were maintained on the FVB/N background (homozygous line 55). Cortico-striatial co-cultures were prepared as previously described (Milnerwood et al., 2012); here striatum neurons were transfected with a GFP-tagged PSD-95 construct or yellow fluorescent protein (YFP) for later identification. The majority of patch clamp electrophysiology and Ca^{2+}-imaging experiments used cortical monocultures plated at a density of 225, 000 neurons/ml; these were otherwise prepared identically to co-cultures (above). In a subset of cortical monoculture experiments, 1 million of the total 2.7 million neurons (plated per 24-well culture) were transfected with transgenic reporters including: GFP; a synaptophysin-tagged GCaMP6-M construct; a postsynaptic density 95 (PSD-95)–tagged M-cherry construct; or a GFP-tagged

internally expressed anti-PSD95 antibody (a generous gift from Dr. D.B. Arnold, University of Southern California(Gross et al., 2013)).

Synaptotagmin-1 Antibody Uptake Assay:

Cortico-striatial co-cultures aged DIV 21 were live-stained with conditioned media containing anti-synaptotagimin-1 (syt-1) antibody (1:00) either in the presence or absence of TTX (500 nM) for various durations (without TTX: 0 min, 5 min, 10 min, 20 min; with TTX: 0 min, 30 min , 60 min and 90 min). Striatal neurons in these cultures expressed either a GFP-tagged PSD-95 construct or YFP (see above). Following anti-syt-1 incubation, cultures were fixed in 10 % paraformaldehyde for a minimum of 15 min, then rinsed 3 times with phosphate buffered saline (PBS). Cultures were subsequently permeabilized with PBS containing 0.1 % triton-X for 5 min and washed 3 times with PBS containing 0.03 % triton-X (PBST). Cultures were then blocked for 45 min in PBST containing 10% normal goat serum (NGS), then incubated overnight at 4 °C in a 1° antibody mixture containing: a chicken anti-GFP/YFP antibody (1:2000) and a guinea pig anti-VGlut-1 antibody (1:4000) in PBST and 2 % NGS. Subsequently cultures were rinsed 3 times with PBST containing 2 % NGS then incubated at room temperature for 2-3 hrs in a 2° antibody mixture containing: an alexa-488 conjugated goat anti-chicken antibody (1:1000) and an AMCA conjugated donkey anti-guinea pig antibody (1:200) in PBST and 2 % NGS. Cultures were then washed 3 times with PBST containing 2 % NGS, then mounted on slides (insert details) with Fluoromount-G (Invitrogen) mounting media.

A maximum of 10 GFP-tagged PSD-95 construct or YFP-labelled striatal neurons were imaged per culture per condition. In all cases, the exposure time for the far-red (syt-1) channel was kept

constant to allow quantitative comparisons of syt-1 fluorescence intensity between cultures and genotypes. Images were exported as Tiffs for analysis in Figi-ImageJ (NIH). GFP-tagged PSD-95 and anti-VGlut-1 puncta (imaged in their respective channels) were thresholded by an analyzer blinded to the culture genotype and condition. VGlut-1 puncta that colocalized with GFP-tagged PSD-95 puncta were selected as ROIs, under which the unprocessed syt-1 fluorescence intensity was measured.

Electrophysiology:

An Axopatch 200B amplifier and pClamp 9.2 software (Molecular Devices, Sunnyvale, CA) were used to acquire whole cell patch clamp electrophysiology recordings. Data was digitized at 20 kHz and low-pass filtered at 1 kHz. For electrophysiology experiments, cultures were perfused with extracellular fluid (ECF) containing (in mM): 167 NaCl, 2.4 KCl, 10 glucose, 10 HEPES, 2 $CaCl_2$ and 1 $MgCl_2$; NaOH (1 mM) was used to adjust the pH to 7.30 with and the osmolarity was adjusted to 305 – 310 mOsm. Tetrodotoxin (TTX) (500 nM) and picrotoxin (PTX) (50 mM) were added to this ECF to block sodium action potentials and $GABA_A$ receptor-mediated currents respectively. Neurons were patched with borosilicate glass pipettes pulled to a tip resistance of 3-6 MΩ when back filled with intracellular solution containing in (mM): 130 Cs-methanesulfonate, 5 CsCl, 4 NaCl, 1 MgCl, 10 HEPES, 5 EGTA, 5 QX-314 Cl, 0.5 Na-GTP, 10 Na-phosphocreatine, and 5 Mg-ATP (~286 mOsm). During experiments, neurons were held at – 70 mV in voltage-clamp, with hyperpolarizing voltage steps (- 10 mV) performed periodically to measure intrinsic membrane properties. Under these conditions AMPA receptor-mediated miniature excitatory post synaptic currents (mEPSC)s appeared as transient inward

current deflections. Recordings with a series resistance greater than 25 MΩ were excluded from analysis; typical values were between 15 – 20 MΩ. A minimum of 2 minutes, following establishment of the whole cell configuration, was allowed before experimental measurements, so neurons could fully dialyze with intracellular solution and achieve a stable membrane resistance and holding current. For experiments involving within-cell drug applications, a maximum 20 % change in series resistance between control and drug measurements was tolerated. In these cases, drugs were applied locally to the neuron with a fast perfusion system. Mini Analysis software (Synaptosoft) was used to detect mEPSC's and extract relevant parameters. A minimum of 100 and no more than 1000 mEPSC's were analysed per neuron per experimental condition.

Cortical Pyramidal Neuron Morphology:

Cortical pyramidal neurons (CPN)s in WT and YAC128 cultures were labeled by transfecting a subset of neurons (1 of 2.7 million) with a cytoplasmic green fluorescent protein (GFP) (add plasmid details) at the time of platting. Cultures were subsequently fixed at DIV-18 and GFP-labeled CPN dendritic arbors imaged on a Zeiss Axiovert 200 M fluorescence microscope (20 x magnification, 0.8 NA), with a Zeiss 702 monochrome camera, using Zen software. Multiple image Z-stacks were acquired and X,Y-tiling was used to ensure entire dendritic arbors were visualized. Images were exported to ImageJ for analysis by a blinded observer. Images were flattened using the maximum Z-projection function. Background subtraction was performed, and neuronal processes were thresholded following adjustment of brightness and contrast. Automated Sholl analysis was performed using the ImageJ sholl analysis plugin.

Synaptophysin -GCaMP Imaging:

We imaged cytosolic Ca^{2+} in axonal boutons of neurons in our cortical mono cultures by transfecting 1 million cells (of a total 2.7 million) at time of plating with a synaptophysin-tagged GCaMP-6m construct (Syn-GCaMP6) created by fusing the full length rat synaptophysin (1-307 amino acids) with GCaMP6m (Chen et al., 2013) through a small linker "GS". The whole synaptophysin-GCaMP6m was the inserted into the pLL3.7-hSyn vector to achieve specific expression in neurons. For some experiments, the same 1 million cells were also transfected at time of platting with an M-cherry-tagged PSD95 construct; in these cases, Syn-GCaMP6-expressing presynaptic boutons colocalized with M-Cherry labeled postsynaptic spines were presumed function synapses.

For all Ca^{2+}-imaging experiments, cultures were platted on 8-well cover-glass chambers (Thermo Scientific ™, Nunc ™, Lab-Tek ™) and imaged at DIV (18) with a Zeiss Axiovert 200 M fluorescence microscope (63 x magnification, 1.4 NA), using a Zeiss 702 monochrome camera and Zen software. Movies were acquired at 10 Hz (100 ms exposure per frame) using the Zen time-series mode with camera-steaming enabled. These experiments were performed in standard ECF (as above) with or without TTX (500 nM) present, but in the absence of PTX.

Spontaneous Ca^{2+} waves were commonly observed in Syn-GCaMP6-labelled axons, evident particularly when action potential-dependent Ca^{2+} events were blocked with TTX. Automatically detecting such Ca^{2+} waves proved difficult with algorithms commonly used to quantify activity-related neuronal GCaMP signals. We therefore, used the Astrocyte Quantitative Analysis

(AQuA) software (running in MATLAB) (Wang et al., 2019) to quantify these waves in the presence of TTX. AQua does not rely on spatially segmenting a Ca^{2+} movie into regions of interest (ROI)s based on neuronal morphology, but rather defines events as spatially and temporally connected Ca^{2+} signals surpassing user-defined thresholds. This means spontaneous axonal waves spreading across multiple boutons are typically classified as a single event, because such Ca^{2+}-activity is grouped in time and space. Conversely, a given bouton can be involved in multiple axonal waves and thus detected as part of multiple events, as long as the pertinent signals are sufficiently temporally separated. To compare the frequency of aQua-detected spontaneous axonal events between genotypes and under pharmacological manipulations, we counted numbers of events occurring within a standardized area [178.6 μm x 113.1 μm (a maximal 63 x field of view)], during a standardized (3 min) consecutive imaging interval. The same aQua detection parameters, empirically determined to best match a small number of manually analyzed experiments, were applied across all cultures and conditions analyzed to facilitate meaningful comparisons.

In a subset of experiments conducted in the presence of TTX, responses of individual WT or YAC128 Syn-GCaMP6-labelled synaptic boutons to caffeine or ionomycin were measured. In these experiments culture fields were imaged for 3 min (as above), after which caffeine (1 mM) or ionomycin (10 μM) was applied and imaging continued for an additional 1-2 min. aQua was not used to analyze these experiments, as an ROI-based algorithm was desired. For caffeine applications, an analyzer (blinded to culture genotype) used Figi-ImageJ (NIH) to manually assign elliptical ROIs to 10 boutons per movie and exported each ROIs fluorescence-intensity time-course. Time-courses were subsequently imported to MATLAB, were the curve fitting tool

was used to model each time-course's photobleaching profile based on the initial 3 min recording; this curve was then extrapolate to the entire time-course including caffeine treatment. The resultant "bleaching curve" was subtracted from the raw Syn-GCaMP6 fluorescence curve and this time-course subsequently divided by the "bleaching curve" to yield a final curve reflecting the caffeine response in DF/F units. Ionomycin experiments were analyzed similarly, except in this case, the blinded analyzer selected 10 active-boutons (showing at least 1 clear Ca^{2+} event during the initial 3 min recording) and 10 inactive-boutons (with no Ca^{2+} events present during the initial 3 min recording). Time-course's derived from inactive-boutons were exported to MATLAB were the ionomycin-mediated DF/F responses were calculated as above. In the case of active-boutons, spontaneous events occurring during the first 3 min were detected with MATLAB's findpeaks function and excised from the raw fluorescence time-courses before curve fitting, but otherwise processed as above.

As expected, spontaneous events were far more frequent when Syn-GCaMP6-expessing cultures where imaged in the absence of TTX. Most boutons showed many events during a 3 min imagining session, which were typically far shorter in duration than TTX-resistant events. These signals, presumably driven by action potential-dependent opening of voltage-gated Ca^{2+} channels, were far more amenable to automated detection algorithms designed to extract action potential driven GCaMP signals from neuronal soma. We therefore used the CaImAn (Flatiron Institute) toolbox in MATLAB (Giovannucci et al., 2019) to analyze these experiments. With CaImAn, we automatically detected active Syn-GCaMP6-expessing boutons, extracted their raw fluorescence signals, removed background fluorescence and calculated corresponding DF/F values. The MATLAB findpeaks function was used to detect events in these DF/F traces and

extract relevant parameters including peak event DF/F amplitudes and event half-amplitude widths. Bouton event frequencies were calculated by dividing numbers of detected events in a DF/F trace by the imaging interval. Bouton event frequencies and event parameters in the absence of TTX were compared between WT and YAC128 cultures under baseline conditions and following application of ryanodine (5 μM).

iGluSnFR Imaging in Acute Brain Slices:

Expression of the genetically-encoded intensity-based glutamate-sensing fluorescence reporter (iGluSnFR) (Marvin et al. 2013) in WT and YAC128 mice was achieved with stereotaxic injection of a viral construct as described previously (Parsons et al., 2016). Briefly, under isoflurane anesthesia, 1 – 1.4 μl of the AAV1.hSyn.iGluSnFr.WPRE.SV40 construct (Penn Vector Core; Dr. Loren Looger, Janelia Farm Research Campus of the Howard Hughes Medical Institute) was directly injected into the dorsal striatum of 4 – 6 week old mice. Following surgery, mice were closely monitored for a week to ensure adequate recovery.

After waiting 3 – 6 weeks, to ensure optimal iGluSnFR expression, acute brain slices from 2-month-old YAC128 mice and age-matched WT controls were prepared as described previously (Parsons et al., 2016; Koch et al., 2018). Briefly, mice were decapitated following deep isoflurane anesthesia and their brains rapidly removed and placed in an ice-cold slicing solution, bubbled with carbogen (95% O_2, 5% CO_2) gas, containing (in mM): 125 NaCl, 2.5 KCl, 25 $NaHCO_3$, 1.25 NaH_2PO_4, 2.5 $MgCl_2$, 0.5 $CaCl_2$, and 10 glucose. 300-μm thick striatum-containing sagittal brain slices were cut with a Leica VT1200S vibratome. Slices were subsequently incubated for 30 min in warmed artificial cerebral spinal fluid ACSF containing 2

mM $CaCl_2$ and 1 mM $MgCl_2$; ACSF constituents and concentrations were otherwise identical to the slicing solution (above).

Slices were transferred to a submerged recording chamber for experiments and perfused with carbogen-bubbled ACSF at a rate of 2 – 3 ml/min at room temperature. Cortical release of glutamate into the striatum was evoked by delivering paired 0.1 ms electrical pulses at 100 Hz with an A-M Systems isolated pulse stimulator (Model 2100) and tungsten monopolar stimulating electrode (tip resistance - 0.1 MΩ). The electrode was placed into a corpus callosum segment adjacent the dorsal striatum at an approximate 50 – 100 μM depth. During and immediately prior to the electrical stimulation, iGluSnR fluorescence was excited with a 470 nm LED; slices were not illuminated between experimental measurements to minimize phototoxicity and bleaching. Stimulation and LED activation were triggered by Clampex software (Molecular Devices, Sunnyvale, CA). iGluSnR fluorescence was isolated with a 530 nm bandpass filter and imaged with a CCD camera (1 M60, Pantera, Dalsa) and XCAP software (Epix, inc.) at 150 Hz with 8 x 8-pixel binning. Experimental measurements encompassing two stimulation trials and one blank trial were performed at 5-minute intervals. The two stimulation trials were averaged and the blank trial, in which slice-fluorescence was imaged without electrical stimulation, was used to account for photobleaching and to calculate the stimulation mediated changes in iGluSnFR fluorescence over basal fluorescence ($\Delta F/F$) as described previously (Parsons et al., 2016). Videos were analyzed offline with ImageJ software. The average iGluSnFR signal was measured over 4 x 4-pixel (93.8 x 93.8 μM) region of interested (ROI) placed over the maximal area of evoked iGSnFR activity within the striatum.

Experimental Design and Statistical Analysis:

Statistical analysis and creation of figures was performed using GraphPad Prism (version 7). All data distributions were tested for normality with the D'Agostino-Pearson omibus normality test.

The Student's unpaired t-test was used for unpaired comparisons between two data groups, such as when mean mEPSC frequencies were compared between WT and YAC128 neurons, as long both data groups were normally distributed. When one or both groups failed the D'Agostino-Pearson omibus normality test, the non-parametric Mann Whitney test was used instead.

When a parameters of the same group of neurons or axonal boutons were compared before and after a drug treatment, statistical significance was assessed with the Student's paired t-test, unless data points in the control or drug-treatment group failed the D'Agostino-Pearson omibus normality test; in which case, the non-parametric Wilcoxon matched-pairs signed rank test was used instead.

A two-way ANOVA with the Bonferroni post-test was used when testing for genotypes difference in a dependent variable measured at different time points, as was the case for our syt-1 antibody uptake and brain-slice iGluSnFR experiments.

Depending on the experimental design, n numbers in figures refer either to number of neurons, numbers of imaged culture fields, numbers of individual axonal bouts, or numbers of brain

slices. Clarifying details are present within individual figure legends, as our numbers of cultures or mice used.

Differences in mean values were considered significant at $p<0.05$, and significance levels are indicated in figures as follows: *$p<0.05$, **$p<0.01$, ***$p<0.001$, ***$p<0.0001$. Comprehensive descriptions of statistical analysis are included in figure legends.

Acknowledgments

We thank Dr. Anne Marie Craig (UBC) for the use of her microscopy equipment and support with the synaptotagmin-1 antibody uptake assay and Lily Zhang for technical support and assistance. The work was supported by funding from the Canadian Institutes of Health Research (CIHR) Foundation grants FDN-143210 to LAR and FDN-154278 to MRH. CB was supported by a University of British Columbia 4-year Graduate Fellowship (UBC 4-YF). ASD was supported by a CIHR Canada Graduate Scholarship Doctoral award and a UBC 4-YF. EK was supported by a CIHR Canada Graduate Scholarship Doctoral award and UBC 4-YF. MES was supported by a Vanier Canada Graduate Scholarship and a University of British Columbia 4-Year Graduate Fellowship. WN was supported by a UBC-CIHR-MD/PhD studentship and a Vanier Canada Graduate Scholarship. LAR holds the UBC Department of Psychiatry Louise A. Brown Chair in Neuroscience. MRH holds a Canada Research Chair.

Figure legends:

Fig 1: Enhanced miniature, but reduced action potential-dependent glutamate release from individual cortical terminals in YAC128 cortical-striatal co-cultures.

A. Fluorescence images from a representative WT cortical-striatal co-culture live-incubated for 30 min with an anti-synaptotagimin-1 (syt-1) antibody conjugated to the Oyster 650 fluorophore in the presence of TTX (500 nM), followed by subsequent fixation and anti-VGLUT-1 immunostaining. The green channel (top left) shows a dendritic segment of a representative striatal spiny projection neuron (SPN) transfected to express a GFP-tagged PSD95 construct labeling dendritic spines. The blue channel (top middle) shows presumed cortical presynaptic terminals labelled by anti-VGLUT-1 immunostaining. The red channel (top right) shows fluorescence intensity associated with anti-synaptotagimin-1 antibody uptake. The bottom channel shows the red, green and blue channels merged; here, colocalized green (PSD95) and blue (VGLUT-1) puncta were interpreted as glutamatergic synapses onto SPNs.

B. Fluorescence images from a representative YAC128 cortical-striatal co-culture stained and represented as in panel **A**. Identical exposure times and excitation illumination intensities were used for imaging anti Syt-1 fluorescence in this panel, panel **A** and all other such experiments. This panel and **A** show an identical segment of syt-1 channels grey-value dynamic range to facilitate meaningful comparisons of the antibody uptake.

C. YAC128 co-cultures showed significantly greater uptake of anti-syt-1 fluorescence at cortical axon terminals synapsing onto SPNs in the presence of TTX (500 nM) (vehicle: n=27 SPNs, Syt1 30 min: n=22 SPNs, Syt1 60 min: n=30 SPNs, Syt1 90 min: n=31 SPNs) (4 culture batches), compared to WT co-cultures (vehicle: n=25 SPNs, Syt1 30 min: n=29 SPNs, Syt1 60

min=28 SPNs, Syt1 90 min=29 SPNs) (3 culture batches), reflecting increased miniature release of glutamate-containing synaptic vesicles. [2-way ANOVA; Genotype: $F(3, 209)= 58.86$, $p<0.0001$; Anti Syt1-incubation time: $F(1, 209)=58.81$, $p<0.0001$; Interaction: $F(3, 209)=10.96$, $p<0.0001$]. Bonferroni's post-test shows significance as indicated.

D. In the absence of TTX, YAC128 co-cultures showed significantly less anti-syt-1 fluorescence uptake at cortical axon terminals synapsing onto SPNs (vehicle: n=51 SPNs, Syt1 5 min: n=43 SPNs, Syt1 10 min: n=50 SPNs, Syt1 20 min: n=51 SPNs) (5 culture batches), compared to WT co-cultures (vehicle: n=44 SPNs, Syt1 5 min: n=43 SPNs, Syt1 10 min=44 SPNs, Syt1 20 min=46 SPNs) (4 culture batches).

Fig 2: YAC128 cortical cultures show elevated miniature EPSC frequencies at early DIV time points.

A. Voltage clamp recordings from representative WT (top) and YAC128 (bottom) cortical pyramidal neurons (CPN)s from day in vitro 7 (DIV-7) cortical cultures at -70 mV in the presence of tetrodotoxin (TTX) (500 nM) and picrotoxin (PTX) (50 μM).

B. The mean CPN miniature excitatory postsynaptic current (mEPSC) frequency at DIV-7 was 1.8 ± 0.3 Hz (n=18, x cultures) in WT CPNs and 2.8 ± 0.7 Hz (n=17) in YAC CPNs; this difference was not statistically significantly [$t(33)=1.449$; $p=0.1567$; Student's unpaired-t test].

C. Mean CPN mEPSC amplitudes at DIV-7 were similar in WT and YAC128 cultures: 17.2 ± 1.5 pA (n=18, x cultures) and 17.0 ± 1.7 pA (n=17) respectively [$t(33)=0.06936$; $p=0.9452$; Student's unpaired-t test].

D. Voltage clamp recordings from representative WT (top) and YAC128 (bottom) cortical pyramidal neurons (CPN)s from day in vitro 14 (DIV-14) cortical cultures at -70 mV in the presence of TTX (500 nM) and PTX (50 μM).

E. The mean CPN mEPSC frequency at DIV-14 was significantly higher in YAC128 cortical cultures [10.8 ± 1.8 Hz (n=20)] compared to WT cultures [4.4 ± 2.6 Hz (n=22, x cultures)], [t(40)=3.555; p=0.0010; Student's unpaired-t test].

F. Mean CPN mEPSC amplitudes at DIV-14 were not significantly different in WT and YAC128 cultures 12.1 ± 0.8 pA (n=22) and 15.0 ± 1.4 pA (n=20, x cultures) respectively [t(40)=1.807; p=0.0786; Student's unpaired-t test].

G. Voltage clamp recordings from representative WT (top) and YAC128 (bottom) cortical pyramidal neurons (CPN)s from day in vitro 18 (DIV-18) cortical cultures at -70 mV in the presence of TTX (500 nM) and PTX (50 μM).

H. The mean CPN mEPSC frequency at DIV-18 was significantly higher in YAC128 cortical cultures [14.1 ± 1.2 Hz (n=38)] compared to WT cultures [9.9 ± 1.5 Hz (n=30, x cultures)], [p<0.0059 (exact); Mann Whitney test].

I. Mean CPN mEPSC amplitudes at DIV-18 were similar in WT and YAC128 cultures: 17.0 ± 1.8 pA (n=30) and 17.4 ± 1.8 pA (n=38) respectively [p=0.8643 (exact); Mann Whitney test].

J. Voltage clamp recordings from representative WT (top) and YAC128 (bottom) cortical pyramidal neurons (CPN)s from day in vitro 21 (DIV-21) cortical cultures at -70 mV in the presence of TTX (500 nM) and PTX (50 μM).

K. The mean CPN mEPSC frequency at DIV-21 was similar in WT and YAC128 cultures: 14.2 ± 1.2 Hz (n=62, x cultures) and 14.0 ± 0.9 Hz (n=71) respectively [p=0.5626 (exact); Mann Whitney test].

L. Mean CPN mEPSC amplitudes at DIV-18 were similar in WT and YAC128 cultures: 22.3 ± 1.3 pA (n=62, x cultures) and 24.3 ± 1.2 pA (n=71) respectively [p=0.2143 (exact); Mann Whitney test].

Fig 3: Dendritic complexity and excitatory synapse numbers are similar in WT and YAC128 cortical cultures.

A. A representative image generated by thresholding a merged Z-stack of a green fluorescent protein (GFP)-expressing WT CPN.

B. A representative image generating by thresholding a merged Z-stack of a GFP-expressing YAC128 CPN.

C. Number of dendritic intersections through concentric sholl circles centered on the soma of GFP-filled WT and YAC128 CPNs of radii between 10 μm and 450 μm. WT and YAC128 CPNs have nearly identical dendritic distributions [2-way ANOVA; Genotype: $F(1, 6165)= 1.168$, $p<0.2799$; Distance from soma: $F(44, 6165)=381.6$, $p<0.0001$; Interaction: $F(44, 6165)=0.9868$, $p<0.4966$].

D. Numbers of sholl intersections, which reflect general neuronal complexity, were similar in WT and YAC128 CPNs: 254.0 ± 8.8 (n=61) and 249.5 ± 8.7 (n=78) respectively [p=0.7263 (exact); Mann Whitney test].

E. A representative merged Z-stack of WT CPN with merged green, red and blue channels showing staining of a genetically-encoded internally-expressed GFP-tagged anti-PSD-95 antibody (green), anti AMPA receptor GluA2 subunit immuno-staining (red) and anti VGLUT-1 immuno-staining (blue) respectively. The bottom panel shows an expanded view of a segment of

dendrite with arrows pointing to a subset of co-localized PSD-95, GluA2 and VGLUT-1 puncta, which were counted as presumed functional synapses. Note, for illustrative purposes the brightness and contrast of the individual channels were adjusted to best illustrate the punctate fluorescence.

F. A representative merged Z-stack of YAC128 CPN with merged green, red and blue channels showing staining of a genetically-encoded internally-expressed GFP-tagged anti-PSD-95 antibody (green), anti AMPA receptor GluA2 subunit immuno-staining (red) and anti VGLUT-1 immuno-staining (blue) respectively. The bottom panel shows an expanded view of a segment of dendrite with arrows pointing to a subset of co-localized PSD-95, GluA2 and VGLUT-1 puncta, which were counted as presumed functional synapses. Note, for illustrative purposes the brightness and contrast of the individual channels were adjusted to best illustrate the punctate fluorescence.

G. Numbers of presumed functional synapses (identified as above) per 100 μm^2 of secondary and tertiary dendrites of WT and YAC128 CPN: 8.8 ± 1.1 (n=37) and 6.8 ± 0.7 (n=57) respectively. Although synapse numbers were lower in YAC128 cultures this did not reach statistical significance [p=0.1039 (exact); Mann Whitney test].

Fig 4: Releasing ER Ca^{2+} with low dose ryanodine increases the pyramidal neuron miniature EPSC frequency in WT, but not YAC128, cultures.

A and B - Hypothetical model (tested below) A. We hypothesize, in wildtype (WT) cultures, spontaneous Ca^{2+} release from ER-stores in presynaptic cortical terminals only minimally augments action potential-independent (mini) glutamate release.

B. Conversely, in YAC128 cultures, we hypothesize spontaneous Ca^{2+} release from presynaptic ER-stores is increased, and that this elevates Ca^{2+}-dependent, mini glutamate release.

C. Voltage clamp recordings from a representative cultured WT cortical pyramidal neuron (CPN) at -70 mV in the presence of tetrodotoxin (TTX) (500 nM) and picrotoxin (PTX) (50 μM), under control conditions (top trace) and during subsequent local ryanodine (5 μM) application (bottom trace). In this CPN, ryanodine (5 μM) substantially increased the mEPSC frequency.

D. Ryanodine (5 μM) significantly increased the mean mEPSC frequency in WT cultured CPNs from 6.7 ± 1.2 Hz to 11.9 ± 2.4 Hz, [t(12)=2.50; p=0.0280; n=13; Student's paired-t test].

E. Ryanodine (5 μM) did not significantly affect the mean WT CPN mEPSC amplitude (control: 21.0 ± 3.2 pA, ryanodine: 20.2 ± 2.3 pA), [t(12)=0.65; p=0.5278; n=13; Student's paired-t test].

F. Voltage clamp recordings from a representative cultured YAC128 CPN (conditions as in panel **C**), under control condition (top trace) and during subsequent local ryanodine (5 μM) application (bottom trace).

G. In YAC128 cultures, ryanodine (5 μM) did not significantly affect the mean CPN mEPSC frequency (control: 12.0 ± 1.7 Hz, ryanodine: 13.9 ± 2.0 Hz), [t(14)=1.65; p=0.1206; n=15; Student's paired-t test].

H. In YAC128 cultures, ryanodine (5 μM) also did not significantly affect the mean CPN mEPSC amplitude (control: 20.5 ± 4.4 pA, ryanodine: 19.6 ± 3.4 pA), [t(14)=0.71; p=0.4904; n=15; Student's paired-t test].

I. Percent change in mEPSC frequency mediated by ryanodine (5 μM) application to WT and YAC128 CPNs (calculated from the responses in panels **D** and **G**). Ryanodine (5 μM) elicited a significantly greater increase in the mEPSC frequency in WT, compared to YAC128, CPNs

[WT: 31.7 ± 7.5 % (n=13), YAC128: 5.2 ± 9.5 % (n=15)], [t(14)=2.141; p=0.0417; Student's unpaired-t test].

Supplemental Fig 1: Releasing ER Ca^{2+} with caffeine the CPN mEPSC frequency in WT, but not YAC128, cultures.

A. Voltage clamp recordings from a representative cultured WT CPN at -70 mV in the presence of TTX (500 nM) and PTX (50 μM), under control conditions (top trace) and during subsequent local caffeine (1 mM) application (bottom trace). In this CPN, caffeine (1 mM) substantially increased the mEPSC frequency.

B. Caffeine (1 mM) significantly increased the mean mEPSC frequency in WT cultured CPNs from 12.3 ± 2.5 Hz to 22.8 ± 8.0 Hz, [p=0.0076 (exact); n=16; Wilcoxon matched-pairs signed rank test].

C. Caffeine (1 mM) did not significantly affect the mean WT CPN mEPSC amplitude (control: 13.7 ± 1.9 pA, caffeine: 17.2 ± 3.4 pA), [p=0.8603 (exact); n=16; Wilcoxon matched-pairs signed rank test].

D. Voltage clamp recordings from a representative cultured YAC128 CPN (conditions as in panel **A**), under control condition (top trace) and during subsequent local caffeine (1 mM) application (bottom trace).

E. In YAC128 cultures, caffeine (1 mM) did not significantly affect the mean CPN mEPSC frequency (control: 12.0 ± 2.1 Hz, caffeine: 11.5 ± 1.9 Hz), [t(12)=0.4808; p=0.6393; n=13; Student's paired-t test].

F. In YAC128 cultures, caffeine (1 mM) also did not significantly affect the mean CPN mEPSC amplitude (control: 14.5 ± 1.4 pA, caffeine: 14.1 ± 1.2 pA), [t(12)=0.8086; p=0.4345; n=13; Student's paired-t test].

G. Percent change in mEPSC frequency mediated by Caffeine (1 mM) application to WT and YAC128 CPNs (calculated from the responses in panels **B** and **E**). Caffeine (1 mM) elicited a significantly greater increase in the mEPSC frequency in WT, compared to YAC128, CPNs [WT: 99.2 ± 34.1 % (n=16, x cultures), YAC128: 1.2 ± 7.6 % (n=13)], [p=0.0025 (exact); Mann Whitney test].

Fig 5: In the presence of CPA and 0 mM extracellular Ca^{2+}, mEPSC are less frequent in YAC128 CPNs than in WT.

A. Voltage clamp recordings from representative WT (top) and YAC128 (bottom) CPNs at -70 mV in the presence of TTX (500 nM) and PTX (50 μM) (as before), with the addition of CPA (30 μM) and in the absence of extracellular Ca^{2+}. Note in all such recording, CPNs were incubated in this CPA-containing, 0 mM Ca^{2+} ECSF for a minimum of 10 min.

B. In CPA (30 μM) and in the absence of extracellular Ca^{2+}, mEPSCs were significantly less frequent in YAC128 CPNs [3.3 ± 0.6 Hz (n=14, x cultures)] compared WT CPNs [8.4 ± 1.5 Hz (n=17)] under like conditions [t(29)=2.952; p=0.0062; Student's unpaired-t test].

C. In CPA (30 μM) and in the absence of extracellular Ca^{2+}, YAC128 CPNs showed a trend towards a lower mean mEPSC amplitude than in WT (WT: 26.7 ± 5.2 pA, YAC128: 16.1 ± 3.3 pA), but this did not reach statistical significance [t(27)=1.706; p=0.0995; Student's unpaired-t test].

Fig 6: Axonal Ca^{2+} waves are more frequent in YAC128 Cortical Cultures.

A. Portion of a WT synapsin-tagged GCaMP-6m (Syn-GCaMP)-expressing axon during a spontaneous Ca^{2+} wave in the presence of ECF containing TTX (500 nM). Images reflect raw GCaMP fluorescence values (arbitrary units) and comprise 15 s of a 4 min video. For illustrative purposes, images were binned temporally from the original 10 Hz movie, such that each 2 s frame reflects the average fluorescence of 20 successively acquired frames.

B. Time course of DF/F (change in fluorescence over basal fluorescence) values extracted from 3 of the WT Syn-GCaMP-expressing axonal boutons (shown in panel **A** with color-coded arrows). Signals were spatially averaged across elliptical regions of interest (ROI)s encompassing the indicated boutons and represent the entire 4 min imaging session. Note the multi-second delay in the propagation of signals between boutons and the long time course of individual events.

C. Numbers of detected spontaneous axonal events (as in Panels **A** and **B**) during 3 min recordings of 63 x objective (178.6 μm x 113.1 μm) fields imaged in the presence of TTX (500 nM). Such action potential-independent events were significantly more frequent in YAC128 cortical cultures [115.9 ± 28.1 events/3 min (n=15 fields, x cultures)], compared to WT [36.3 ± 5.5 events/3 min (n=12 fields)], [p=0.0016 (exact); Mann Whitney test].

D. Average peak DF/F amplitudes of all the spontaneous, action potential-independent axonal Ca^{2+} events imaged in a given 63 x objective field over 3 min from WT and YAC128 cortical cultures. Average event amplitudes were not significantly different between WT [0.240 ± 0.046 DF/F (n=10 fields, x cultures)] and YAC128 cultures [0.216 ± 0.027 DF/F (n=12 fields)], [t(20)=0.465; p=0.647; Student's unpaired-t test].

Fig 7: Boutons spontaneously active in TTX show relatively elevated cytosolic Ca^{2+} in both genotypes. Resting cytosolic Ca^{2+} concentrations are higher in the overall YAC128 bouton population.

A. DF/F time courses from two Syn-GCaMP-expressing axonal boutons from a representative YAC128 culture in the presence of TTX (500 nM). The first bouton (top trace) is inactive during the 3 min imaging session, while the second bouton (bottom trace) shows a clear spontaneous event (black arrow). Subsequent application of the Ca^{2+} ionophore ionomycin (10 μM) elicits a smaller Ca^{2+} response in the spontaneously active bouton, suggesting a higher basal cytosolic Ca^{2+} concentration (pre-ionomycin) in the active bouton.

B. Ionomycin responses of WT Syn-GCaMP-expressing boutons in the presence of TTX following a 3 min imaging session. Boutons were classified as active or inactive based on the presence, or lack thereof, at least one spontaneous Ca^{2+} event during the initial 3 minute recording. Ionomycin responses were significantly larger in the population of inactive boutons [0.633 ± 0.072 DF/F (n=67 boutons, x cultures)], vs active boutons [0.191 ± 0.026 DF/F (n=41 boutons)], [$p<0.0001$ (exact); Mann Whitney test].

C. Ionomycin responses of YAC128 Syn-GCaMP-expressing boutons in the presence of TTX following a 3 min imaging session as in panel **B**. Ionomycin responses were significantly larger in the population of inactive boutons [0.410 ± 0.040 DF/F (n=51 boutons)], vs active boutons [0.149 ± 0.016 DF/F (n=46 boutons, x cultures)], [$p<0.0001$ (exact); Mann Whitney test].

D. Responses of Syn-GCaMP-expressing axons from a representative WT cortical culture to ionomycin (10 μM). Images are from a 4 min imaging session, with ionomycin application at 3 min and reflect raw GCaMP fluorescence values (arbitrary units) (as above). To minimize impacts of photobleaching, the top (before) image is the frame immediately prior ionomycin.

The bottom image is a maximum projection of all frames acquired 30s prior and following ionomycin treatment and reflect each pixel's maximum ionomycin response.

E. Responses of Syn-GCaMP-expressing axons from a representative YAC128 cortical culture to ionomycin (10 μM). As above, the top (before) image is the frame immediately prior ionomycin. The bottom image is a maximum projection of all frames acquired 30s prior and following ionomycin and reflect each pixel's maximum ionomycin response. The visible grey-value dynamic range is the same as in panel **D**, (150 increments of the total unprocessed 14 bit-depth), however the 0 value has been adjusted so that brightness of the before image is comparable to that of its WT counterpart in **D**; this is so the reader can better appreciate the YAC128 culture's smaller relative change in fluorescence.

F. Ionomycin responses of the all WT and YAC128 Syn-GCaMP-expressing axons automatically detected with the aQua software suite (see methods for reference). The WT bouton population showed a significantly greater ionomycin-mediated change in fluorescence [0.272 ± 0.006 DF/F (n=1681 boutons, x cultures)] compared to the YAC128 population [0.190 ± 0.002 DF/F (n=1462 boutons)], [$p<0.0001$ (exact); Mann Whitney test].

Fig 8: Caffeine increases the frequency of spontaneous Ca^{2+} events and the resting Ca^{2+} concentration in WT, but not YAC128, cortical axonal boutons.

A. Numbers of detected spontaneous Syn-GCaMP axonal events in the presence TTX (500 nM) during 3 min recordings of 63 x objective fields of WT cortical cultures (as above). The control group consists of the same WT culture fields shown in **(Figure 6: C)**, and is compared to separate WT culture fields imaged in the presence of caffeine (1 mM) under otherwise like conditions. WT axons showed significantly more action potential-independent events in the

presence of caffeine, than in its absence [203.8 ± 55.2 events/3 min (n=10 fields)] vs [36.3 ± 5.5 events/3 min (n=12 fields)] respectively [t(20)=3.316; p=0.0034; Student's unpaired-t test].

B. Numbers of detected spontaneous Syn-GCaMP axonal events in the presence TTX (500 nM) during 3 min recordings of 63 x objective fields of YAC128 cortical cultures (as above). The control group consists of the same YAC128 culture fields shown in **(Figure 6: C)**, and is compared to separate YAC128 culture fields imaged in the presence of caffeine (1 mM) under otherwise like conditions. Numbers of detected YAC128 axonal events were not significantly different in the presence or absence of caffeine [115.1 ± 28.21 events/3 min (n=15 fields)] vs [150.0 ± 28.55 events/3 min (n=8 fields)] respectively [p=0.2188 (exact); Mann Whitney test].

C. DF/F time courses from representative WT (top) and YAC128 (bottom) Syn-GCaMP-expressing axonal boutons in the presence of TTX (500 nM) before and immediately following application of caffeine (1 mM). For this illustration, boutons were selected which did not show spontaneous events. Rather, note the gradual sustained increase in Syn-GCaMP fluorescence, which is of larger magnitude in the WT bouton.

D. Caffeine responses of WT and YAC128 Syn-GCaMP-expressing boutons in the presence of TTX as illustrated in panel **C.** Boutons showing spontaneous events **(as in Figure 6)** were excluded as the long time course of such events complicated quantification of steady-state increases in DF/F. Caffeine application elicited a significantly greater increase in Syn-GCaMP fluorescence in WT boutons [0.342 ± 0.030 DF/F (n=87 boutons)] compared to YAC128 [0.229 ± 0.039 DF/F (n=54 boutons)] [p=0.0004 (exact); Mann Whitney test].

Fig 9: In the absence of TTX, presynaptic calcium events are more frequent and of longer duration in WT, compared to YAC128, cultures.

A. DF/F time course from representative WT Syn-GCaMP-expressing axonal bouton in the absence of TTX. The expanded time course (right) illustrates the relatively long width of these action potential-dependent events.

B. DF/F time course from representative YAC128 Syn-GCaMP-expressing axonal bouton in the absence of TTX. The expanded time course (right) illustrates the shorter time course of the action potential-dependent events compared to WT (above).

C. Frequencies of spontaneous events in WT an YAC128 Syn-GCaMP-expressing axonal boutons in the absence of TTX. Event frequencies were significantly higher in WT boutons.

D. Mean half-peak widths of the spontaneous events detected in WT and YAC128 Syn-GCaMP-expressing axonal boutons during 3 min imaging sessions in the absence of TTX. The duration of such event was significantly longer in WT boutons.

Fig 10: Ryanodine reduces evoked striatal iGluSnR responses in WT, but not YAC128, brain slices and .

A. Image of raw iGluSnR fluorescence from a representative WT mouse brain slice with viral-mediated expression of iGluSnR in its dorsal striatum. Note the square ROI over which evoked spatially averaged DF/F signals were measured and the tungsten monopolar stimulating electrode placed in the corpus callosum.

B. A DF/F image montage from the above WT brain slice, illustrating a striatum iGluSnR response evoked by electrically stimulating cortical axons in the adjacent corpus callosum.

C. Striatum evoked DF/F iGluSnR responses from a representative WT (top) and YAC128 Bottom) brain slice before and in the presence of ryanodine (5 μM). Ryanodine elicits a substantial reduction in the peak WT, but not YAC128, iGluSnR response.

D. Peak evoked striatum iGluSnR responses from WT and YAC128 slices before and after treatment of slices with ryanodine (5 μM). Responses were measure repeatedly at 3 min intervals and were normalized to the average of each slices 3 baseline (before drug) measurements. Ryanodine application decreased the amplitude of the evoked iGluSnR response in WT (n=9 slices, x mice), but not YAC128 (n=8) slices. The effect of ryanodine on WT slices slice was significantly than in YAC128, slice base on a significant time, genotype interaction (p=0.0094, repeated measure (time) two way ANOVA).

References

Anon (1993) A novel gene containing a trinucleotide repeat that is expanded and unstable on Huntington“s disease chromosomes. The Huntington”s Disease Collaborative Research Group. Cell 72:971–983.

Atasoy D, Ertunc M, Moulder KL, Blackwell J, Chung C, Su J, Kavalali ET (2008) Spontaneous and evoked glutamate release activates two populations of NMDA receptors with limited overlap. J Neurosci 28:10151–10166.

Bachoud-Lévi A-C, Ferreira J, Massart R, Youssov K, Rosser A, Busse M, Craufurd D, Reilmann R, De Michele G, Rae D, Squitieri F, Seppi K, Perrine C, Scherer-Gagou C, Audrey O, Verny C, Burgunder J-M (2019) International Guidelines for the Treatment of Huntington's Disease. Front Neurol 10:710.

Beal MF, Kowall NW, Ellison DW, Mazurek MF, Swartz KJ, Martin JB (1986) Replication of the neurochemical characteristics of Huntington's disease by quinolinic acid. Nature 321:168–171.

Beaulieu-Laroche L, Harnett MT (2018) Dendritic Spines Prevent Synaptic Voltage Clamp. Neuron 97:75–82.e3.

Botelho EP, Wang E, Chen JY, Holley S, Andre V, Cepeda C, Levine MS (2014) Differential Synaptic and Extrasynaptic Glutamate-Receptor Alterations in Striatal Medium-Sized Spiny Neurons of Aged YAC128 Huntington's Disease Mice. PLoS Currents 6.

Budde T, Meuth S, Pape H-C (2002) Calcium-dependent inactivation of neuronal calcium channels. Nat Rev Neurosci 3:873–883.

Buren C, Parsons MP, Smith-Dijak A, Raymond LA (2016) Impaired development of cortico-striatal synaptic connectivity in a cell culture model of Huntington's disease. Neurobiol Dis 87:80–90.

Cens T, Rousset M, Leyris J-P, Fesquet P, Charnet P (2006) Voltage- and calcium-dependent inactivation in high voltage-gated Ca(2+) channels. Prog Biophys Mol Biol 90:104–117.

Cepeda C, Hurst RS, Calvert CR, Hernández-Echeagaray E, Nguyen OK, Jocoy E, Christian LJ, Ariano MA, Levine MS (2003) Transient and progressive electrophysiological alterations in the corticostriatal pathway in a mouse model of Huntington's disease. J Neurosci 23:961–969.

Chen T-W, Wardill TJ, Sun Y, Pulver SR, Renninger SL, Baohan A, Schreiter ER, Kerr RA, Orger MB, Jayaraman V, Looger LL, Svoboda K, Kim DS (2013) Ultrasensitive fluorescent proteins for imaging neuronal activity. Nature 499:295–300.

de Juan-Sanz J, Holt GT, Schreiter ER, de Juan F, Kim DS, Ryan TA (2017) Axonal Endoplasmic Reticulum Ca 2+ Content Controls Release Probability in CNS Nerve Terminals. Neuron 93:867–881.e6.

Emptage NJ, Reid CA, Fine A (2001) Calcium Stores in Hippocampal Synaptic Boutons Mediate Short-Term Plasticity, Store-Operated Ca2+ Entry, and Spontaneous Transmitter Release. Neuron 29:197–208.

Espinosa F, Kavalali ET (2009) NMDA Receptor Activation by Spontaneous Glutamatergic Neurotransmission. J Neurophysiol 101:2290–2296.

Fernández-Chacón R, Königstorfer A, Gerber SH, García J, Matos MF, Stevens CF, Brose N, Rizo J, Rosenmund C, Südhof TC (2001) Synaptotagmin I functions as a calcium regulator of release probability. Nature 410:41–49.

Frank CA, Kennedy MJ, Goold CP, Marek KW, Davis GW (2006) Mechanisms underlying the rapid induction and sustained expression of synaptic homeostasis. Neuron 52:663–677.

Fredj NB, Burrone J (2009) A resting pool of vesicles is responsible for spontaneous vesicle fusion at the synapse. Nat Neurosci 12:751–758.

Geppert M, Goda Y, Hammer RE, Li C, Rosahl TW, Stevens CF, Südhof TC (1994) Synaptotagmin I: a major Ca2+ sensor for transmitter release at a central synapse. Cell 79:717–727.

Giovannucci A, Friedrich J, Gunn P, Kalfon J, Brown BL, Koay SA, Taxidis J, Najafi F, Gauthier JL, Zhou P, Khakh BS, Tank DW, Chklovskii DB, Pnevmatikakis EA (2019) CaImAn an open source tool for scalable calcium imaging data analysis. Elife 8:413.

Graveland GA, Williams RS, DiFiglia M (1985) Evidence for degenerative and regenerative changes in neostriatal spiny neurons in Huntington's disease. Science 227:770–773.

Gross GG, Junge JA, Mora RJ, Kwon H-B, Olson CA, Takahashi TT, Liman ER, Ellis-Davies GCR, McGee AW, Sabatini BL, Roberts RW, Arnold DB (2013) Recombinant probes for visualizing endogenous synaptic proteins in living neurons. Neuron 78:971–985.

Hantraye P, Riche D, Maziere M, Isacson O (1990) A primate model of Huntington's disease: behavioral and anatomical studies of unilateral excitotoxic lesions of the caudate-putamen in the baboon. Exp Neurol 108:91–104.

Joshi PR, Wu N-P, André VM, Cummings DM, Cepeda C, Joyce JA, Carroll JB, Leavitt BR, Hayden MR, Levine MS, Bamford NS (2009) Age-dependent alterations of corticostriatal activity in the YAC128 mouse model of Huntington disease. J Neurosci 29:2414–2427.

Kavalali ET (2015) The mechanisms and functions of spontaneous neurotransmitter release. Nat Rev Neurosci 16:5–16.

Llano I, González J, Caputo C, Lai FA, Blayney LM, Tan YP, Marty A (2000) Presynaptic calcium stores underlie large-amplitude miniature IPSCs and spontaneous calcium transients. Nat Neurosci 3:1256–1265.

McKinney RA, Capogna M, Dürr R, Gähwiler BH, Thompson SM (1999) Miniature synaptic events maintain dendritic spines via AMPA receptor activation. Nat Neurosci 2:44–49.

Meissner G (2017) The structural basis of ryanodine receptor ion channel function. J Gen Physiol 149:1065–1089.

Miller BR, Dorner JL, Shou M, Sari Y, Barton SJ, Sengelaub DR, Kennedy RT, Rebec GV (2008) Up-regulation of GLT1 expression increases glutamate uptake and attenuates the Huntington's disease phenotype in the R6/2 mouse. Neuroscience 153:329–337.

Milnerwood AJ, Gladding CM, Pouladi MA, Kaufman AM, Hines RM, Boyd JD, Ko RWY, Vasuta OC, Graham RK, Hayden MR, Murphy TH, Raymond LA (2010) Early Increase in Extrasynaptic NMDA Receptor Signaling and Expression Contributes to Phenotype Onset in Huntington's Disease Mice. Neuron 65:178–190.

Milnerwood AJ, Kaufman AM, Sepers MD, Gladding CM, Zhang L, Wang L, Fan J, Coquinco A, Qiao JY, Lee H, Wang YT, Cynader M, Raymond LA (2012) Mitigation of augmented extrasynaptic NMDAR signaling and apoptosis in cortico-striatal co-cultures from Huntington's disease mice. Neurobiol Dis 48:40–51.

Parsons MP, Vanni MP, Woodard CL, Kang R, Murphy TH, Raymond LA (2016) Real-time imaging of glutamate clearance reveals normal striatal uptake in Huntington disease mouse models. Nat Commun 7:11251.

Peled ES, Newman ZL, Isacoff EY (2014) Evoked and spontaneous transmission favored by distinct sets of synapses. Curr Biol 24:484–493.

Raymond LA, André VM, Cepeda C, Gladding CM, Milnerwood AJ, Levine MS (2011) Pathophysiology of Huntington's disease: time-dependent alterations in synaptic and receptor function. Neuroscience 198:252–273.

Ross WN (2012) Understanding calcium waves and sparks in central neurons. Nat Rev Neurosci 13:157–168.

Sara Y, Virmani T, Deák F, Liu X, Kavalali ET (2005) An isolated pool of vesicles recycles at rest and drives spontaneous neurotransmission. Neuron 45:563–573.

Sepers MD, Smith-Dijak A, LeDue J, Kolodziejczyk K, Mackie K, Raymond LA (2017) Endocannabinoid-specific impairment in synaptic plasticity in striatum of Huntington's disease mouse model. J Neurosci:1739–17.

Sutton MA, Ito HT, Cressy P, Kempf C, Woo JC, Schuman EM (2006) Miniature neurotransmission stabilizes synaptic function via tonic suppression of local dendritic protein synthesis. Cell 125:785–799.

Sutton MA, Taylor AM, Ito HT, Pham A, Schuman EM (2007) Postsynaptic decoding of neural activity: eEF2 as a biochemical sensor coupling miniature synaptic transmission to local protein synthesis. Neuron 55:648–661.

Suzuki M, Nagai Y, Wada K, Koike T (2012) Calcium leak through ryanodine receptor is involved in neuronal death induced by mutant huntingtin. Biochem Biophys Res Commun 429:18–23.

Tang T-S, Tu H, Chan EYW, Maximov A, Wang Z, Wellington CL, Hayden MR, Bezprozvanny I (2003) Huntingtin and huntingtin-associated protein 1 influence neuronal calcium signaling mediated by inositol-(1,4,5) triphosphate receptor type 1. Neuron 39:227–239.

Tang TS, Guo C, Wang H, Chen X, Bezprozvanny I (2009) Neuroprotective Effects of Inositol 1,4,5-Trisphosphate Receptor C-Terminal Fragment in a Huntington's Disease Mouse Model. Journal of Neuroscience 29:1257–1266.

Tyebji S, Hannan AJ (2017) Synaptopathic mechanisms of neurodegeneration and dementia: Insights from Huntington's disease. Prog Neurobiol 153:18–45.

Vonsattel JP, Myers RH, Stevens TJ, Ferrante RJ, Bird ED, Richardson EP (1985) Neuropathological classification of Huntington's disease. J Neuropathol Exp Neurol 44:559–577.

Wang R, Reddy PH (2017) Role of Glutamate and NMDA Receptors in Alzheimer's Disease. J Alzheimers Dis 57:1041–1048.

Wang Y, DelRosso NV, Vaidyanathan TV, Cahill MK, Reitman ME, Pittolo S, Mi X, Yu G, Poskanzer KE (2019) Accurate quantification of astrocyte and neurotransmitter fluorescence dynamics for single-cell and population-level physiology. Nat Neurosci 22:1936–1944.

Xu J, Pang ZP, Shin O-H, Südhof TC (2009) Synaptotagmin-1 functions as a Ca2+ sensor for spontaneous release. Nat Neurosci 12:759–766.

Figure 1:

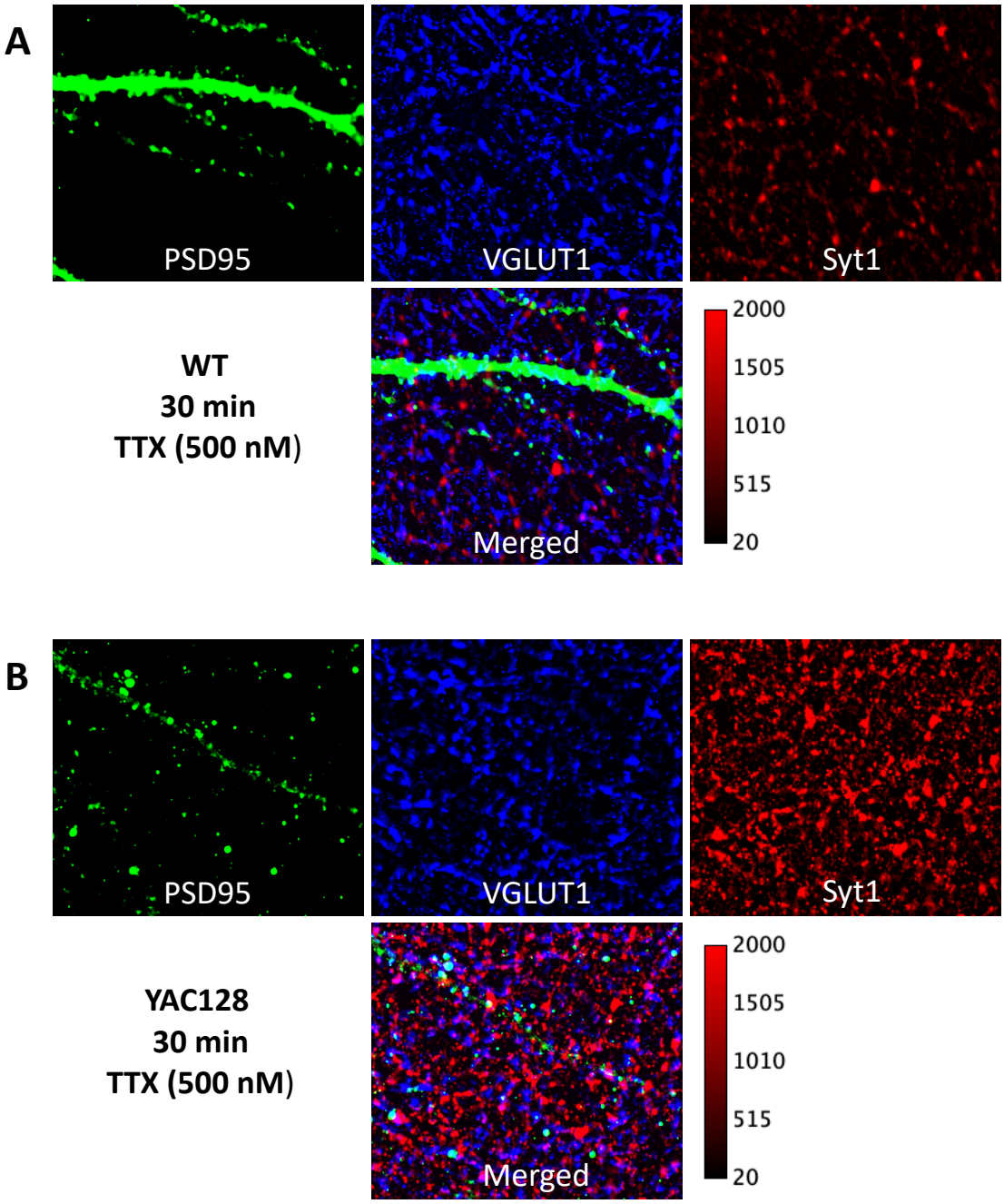
A
PSD95
VGLUT1
Syt1
WT
30 min
TTX (500 nM)
Merged
2000
1505
1010
515
20
B
PSD95
VGLUT1
Syt1
YAC128
30 min
TTX (500 nM)
Merged
2000
1505
1010
515
20

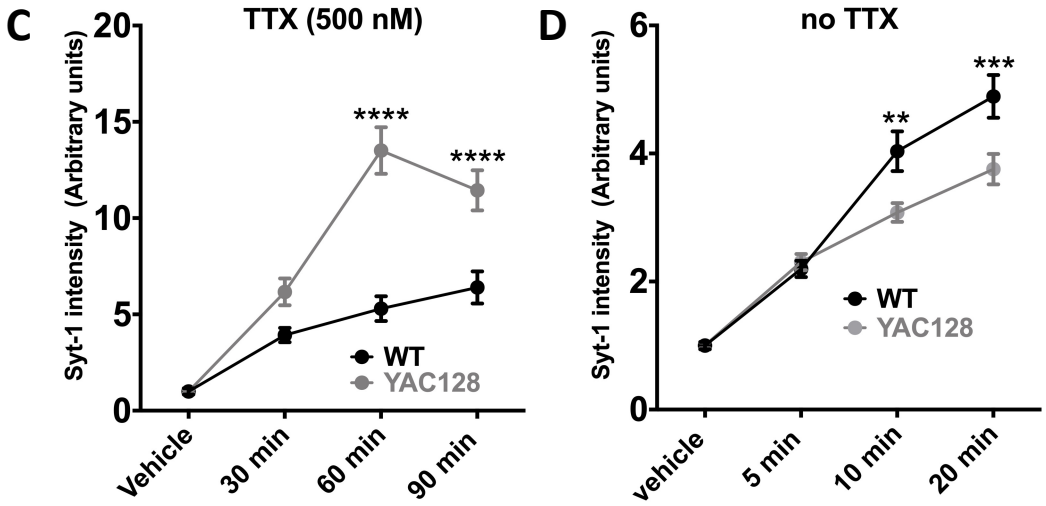
C
TTX (500 nM)
Syt-1 intensity (Arbitrary units)
20
15
10
5
0
****
****
WT
YAC128
Vehicle
30 min
60 min
90 min
D
no TTX
Syt-1 intensity (Arbitrary units)
6
4
2
0
**
***
WT
YAC128
vehicle
5 min
10 min
20 min

Figure 2:

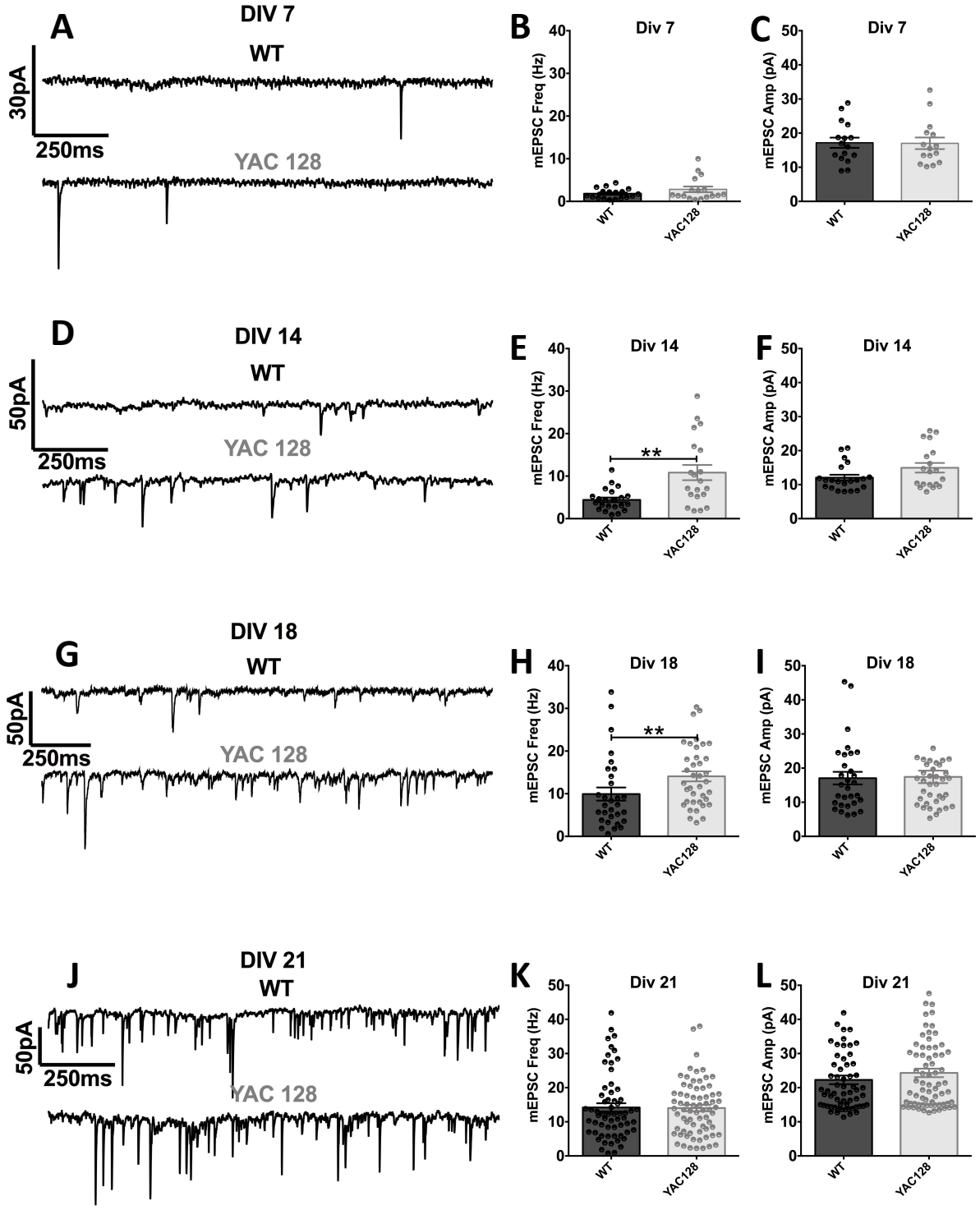
A
DIV 7
WT
30pA
250ms
YAC 128
B
Div 7
mEPSC Freq (Hz)
WT
YAC128
C
Div 7
mEPSC Amp (pA)
WT
YAC128
D
DIV 14
WT
50pA
250ms
YAC 128
E
Div 14
mEPSC Freq (Hz)
**
WT
YAC128
F
Div 14
mEPSC Amp (pA)
WT
YAC128
G
DIV 18
WT
50pA
250ms
YAC 128
H
Div 18
mEPSC Freq (Hz)
**
WT
YAC128
I
Div 18
mEPSC Amp (pA)
WT
YAC128
J
DIV 21
WT
50pA
250ms
YAC 128
K
Div 21
mEPSC Freq (Hz)
WT
YAC128
L
Div 21
mEPSC Amp (pA)
WT
YAC128

Figure 3:

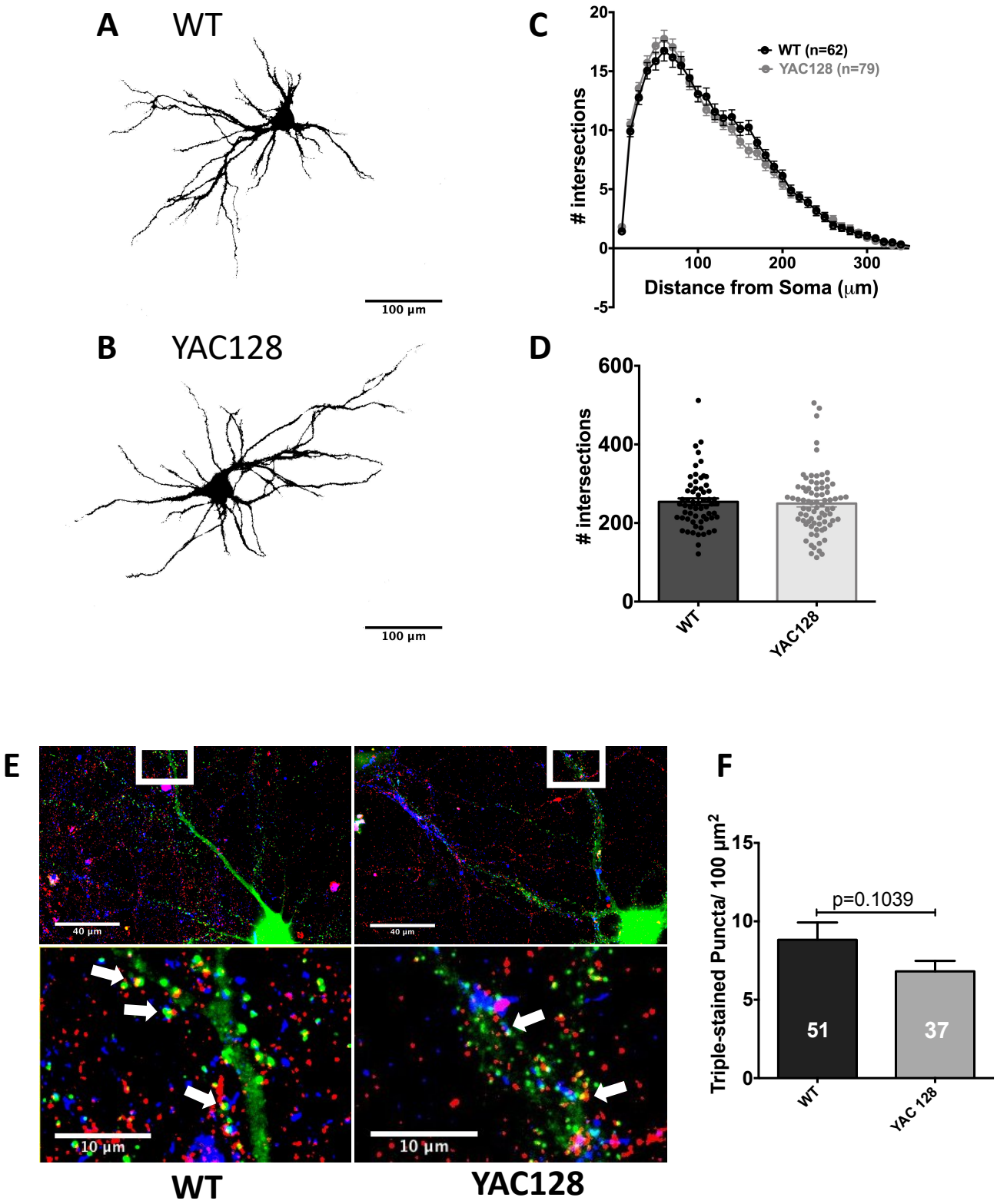
A
WT
100 µm
B
YAC128
100 µm
C
WT (n=62)
YAC128 (n=79)
intersections
Distance from Soma (µm)
D
intersections
WT
YAC128
E
40 µm
10 µm
WT
YAC128
F
Triple-stained Puncta/ 100 µm²
p=0.1039
51
37
WT
YAC 128

Figure 4:

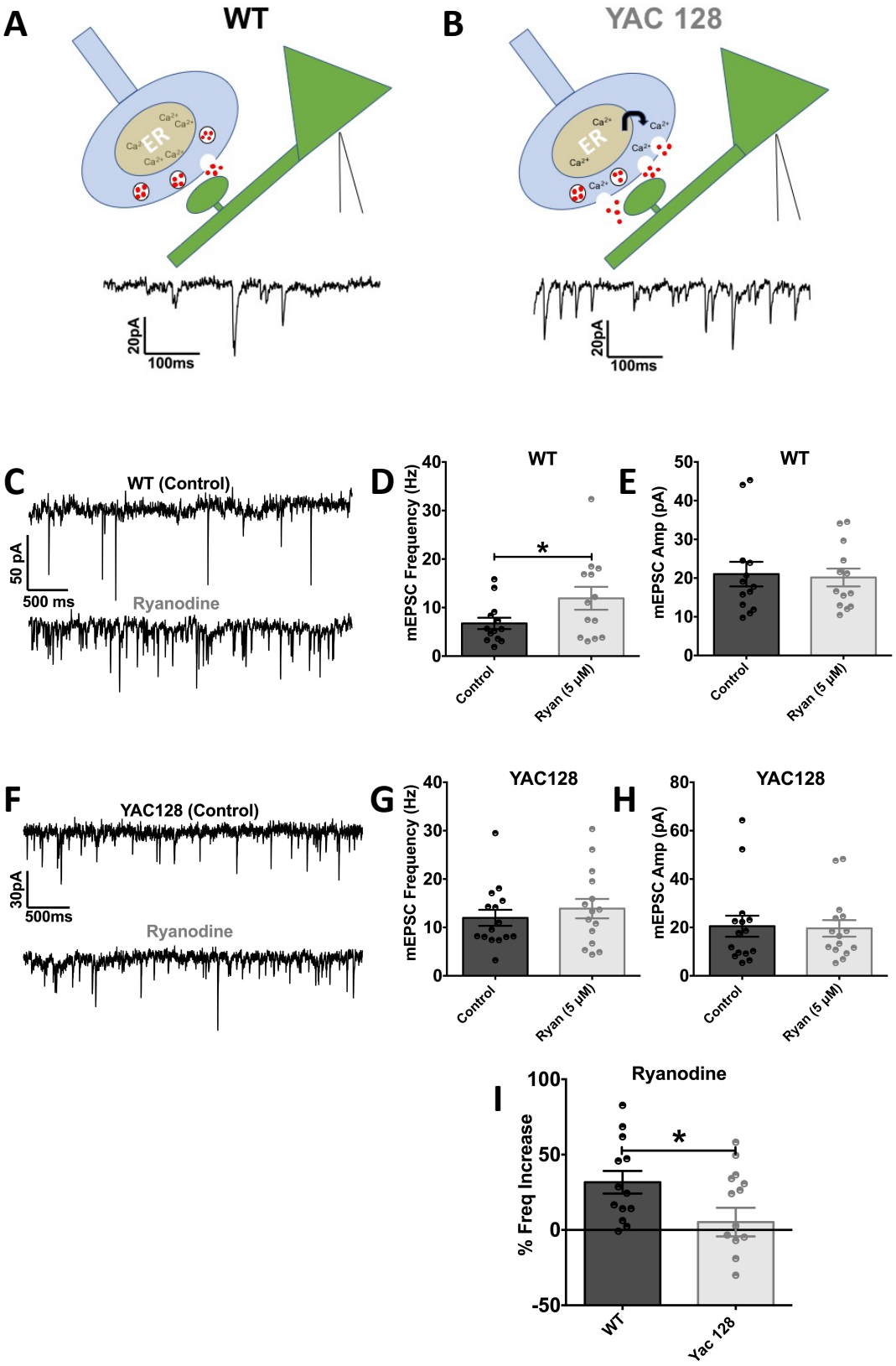
A
WT
ER
20pA
100ms
B
YAC 128
ER
20pA
100ms
C
WT (Control)
50 pA
500 ms
Ryanodine
D
WT
mEPSC Frequency (Hz)
Control
Ryan (5 μM)
E
WT
mEPSC Amp (pA)
Control
Ryan (5 μM)
F
YAC128 (Control)
30pA
500ms
Ryanodine
G
YAC128
mEPSC Frequency (Hz)
Control
Ryan (5 μM)
H
YAC128
mEPSC Amp (pA)
Control
Ryan (5 μM)
I
Ryanodine
% Freq Increase
WT
Yac 128

Supplemental Figure 1:

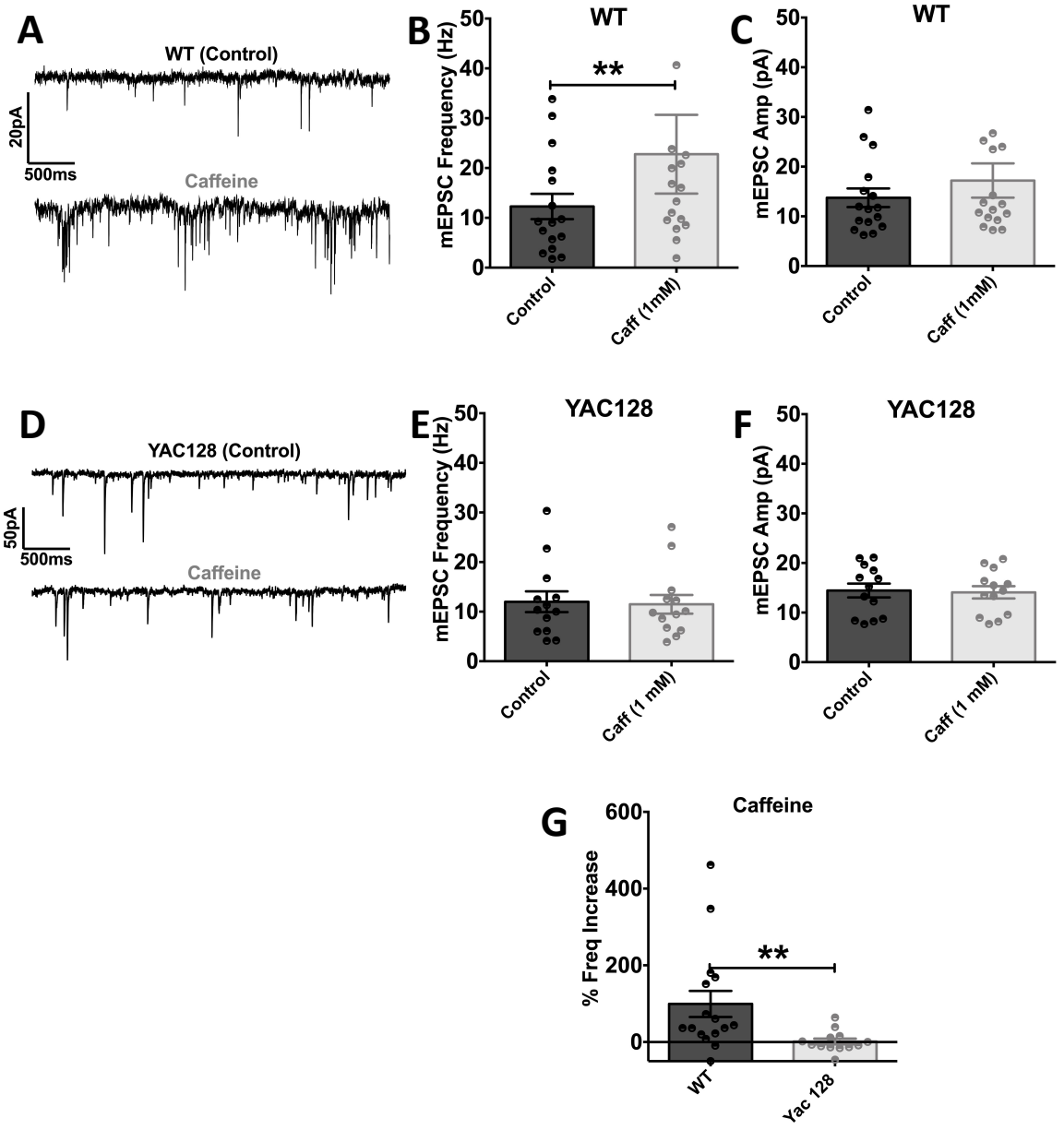

Figure 5:

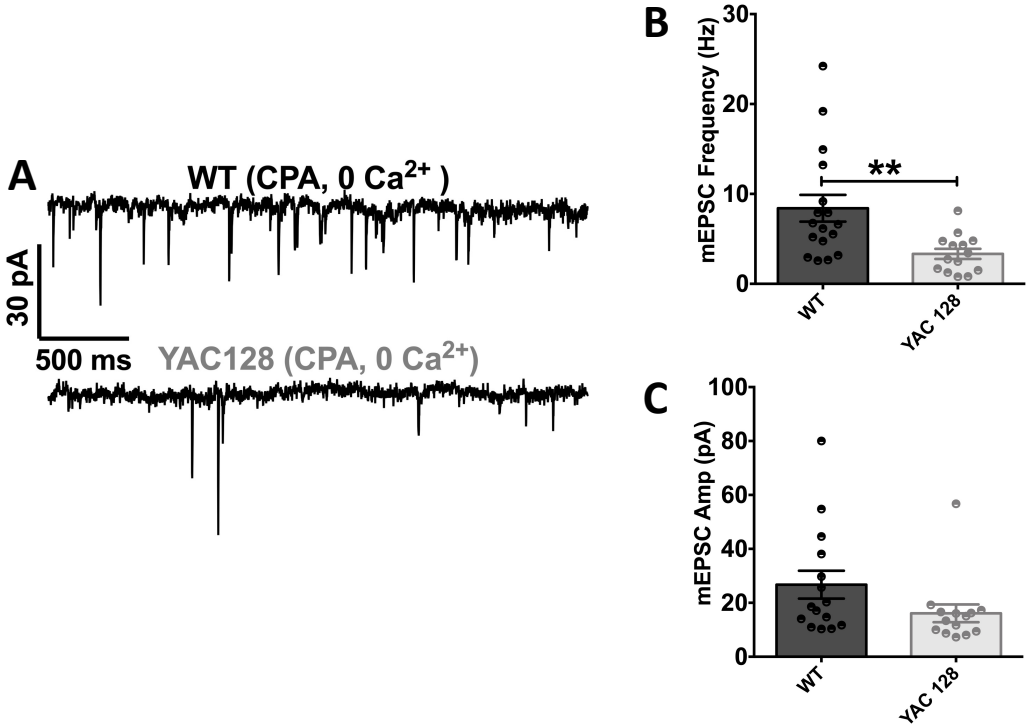
A
WT (CPA, 0 Ca2+)
30 pA
500 ms
YAC128 (CPA, 0 Ca2+)
B
mEPSC Frequency (Hz)
30
20
10
0
**
WT
YAC 128
C
mEPSC Amp (pA)
100
80
60
40
20
0
WT
YAC 128

Figure 6:

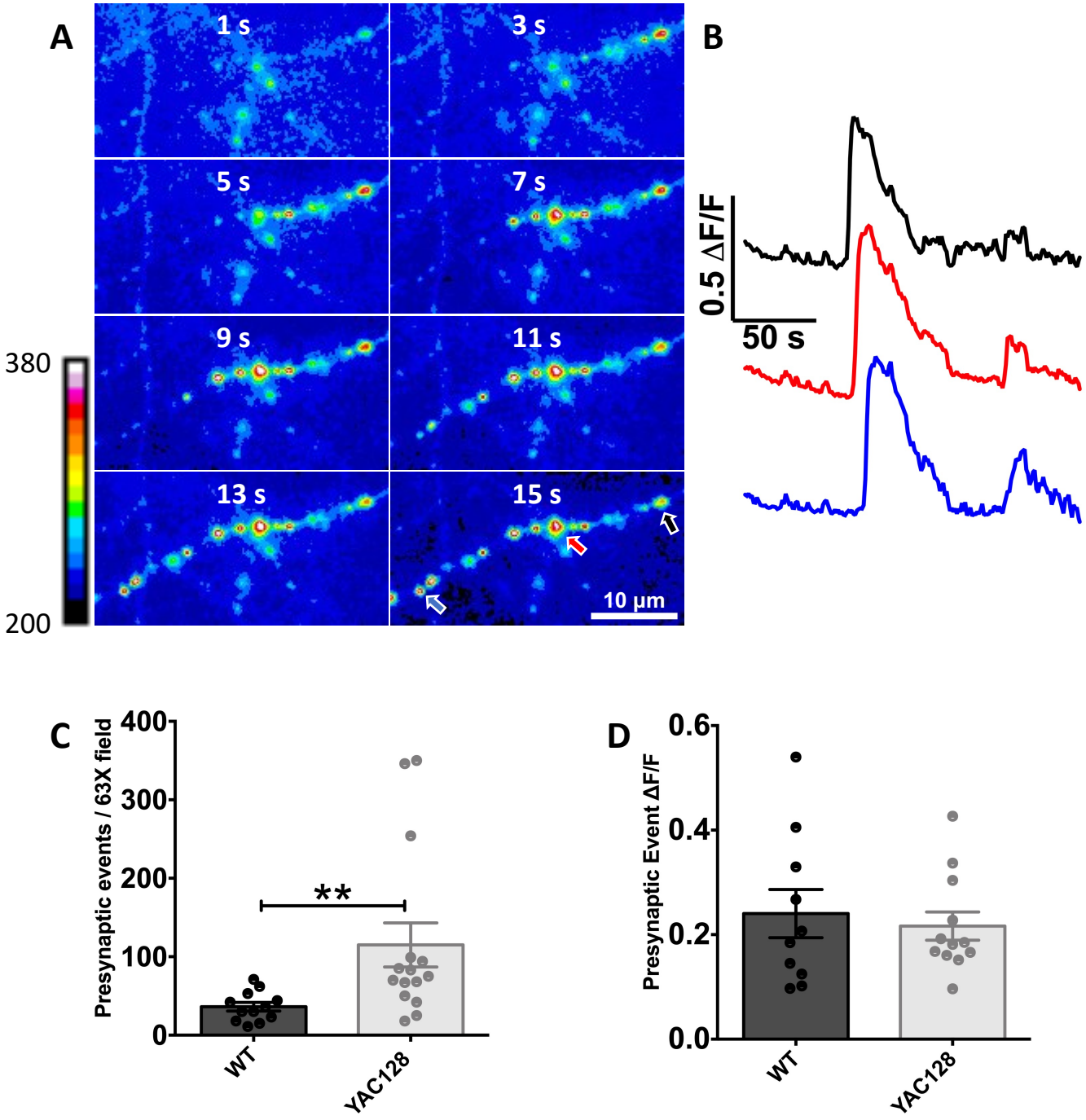
A
1 s
3 s
5 s
7 s
9 s
11 s
13 s
15 s
10 µm
380
200
B
0.5 ΔF/F
50 s
C
Presynaptic events / 63X field
400
300
200
100
0
**
WT
YAC128
D
Presynaptic Event ΔF/F
0.6
0.4
0.2
0.0
WT
YAC128

Figure 7:

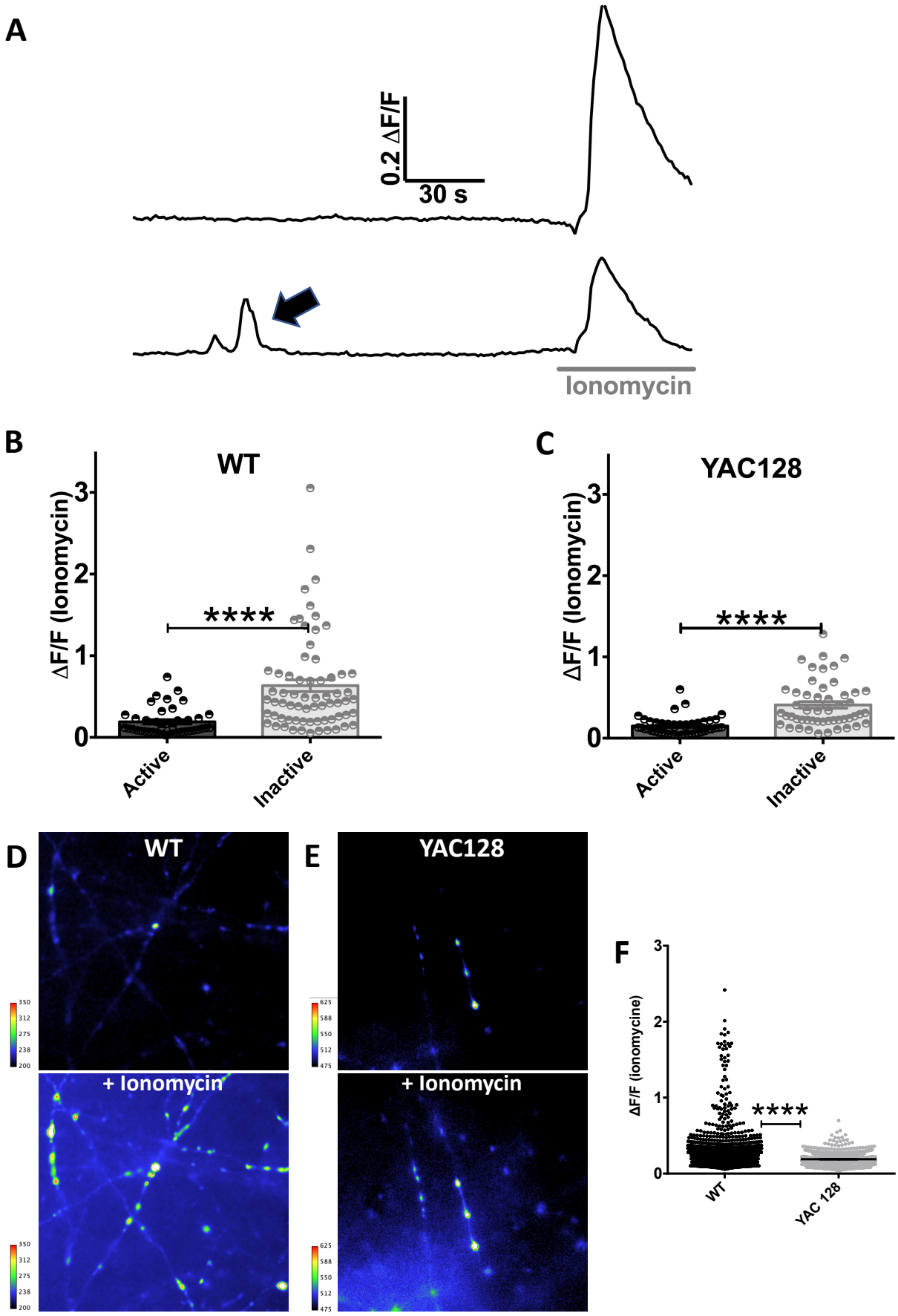
A
0.2 ΔF/F
30 s
Ionomycin
B
WT
ΔF/F (Ionomycin)
****
Active
Inactive
C
YAC128
ΔF/F (Ionomycin)
****
Active
Inactive
D
WT
+ Ionomycin
E
YAC128
+ Ionomycin
F
ΔF/F (ionomycine)
****
WT
YAC 128

Figure 8:

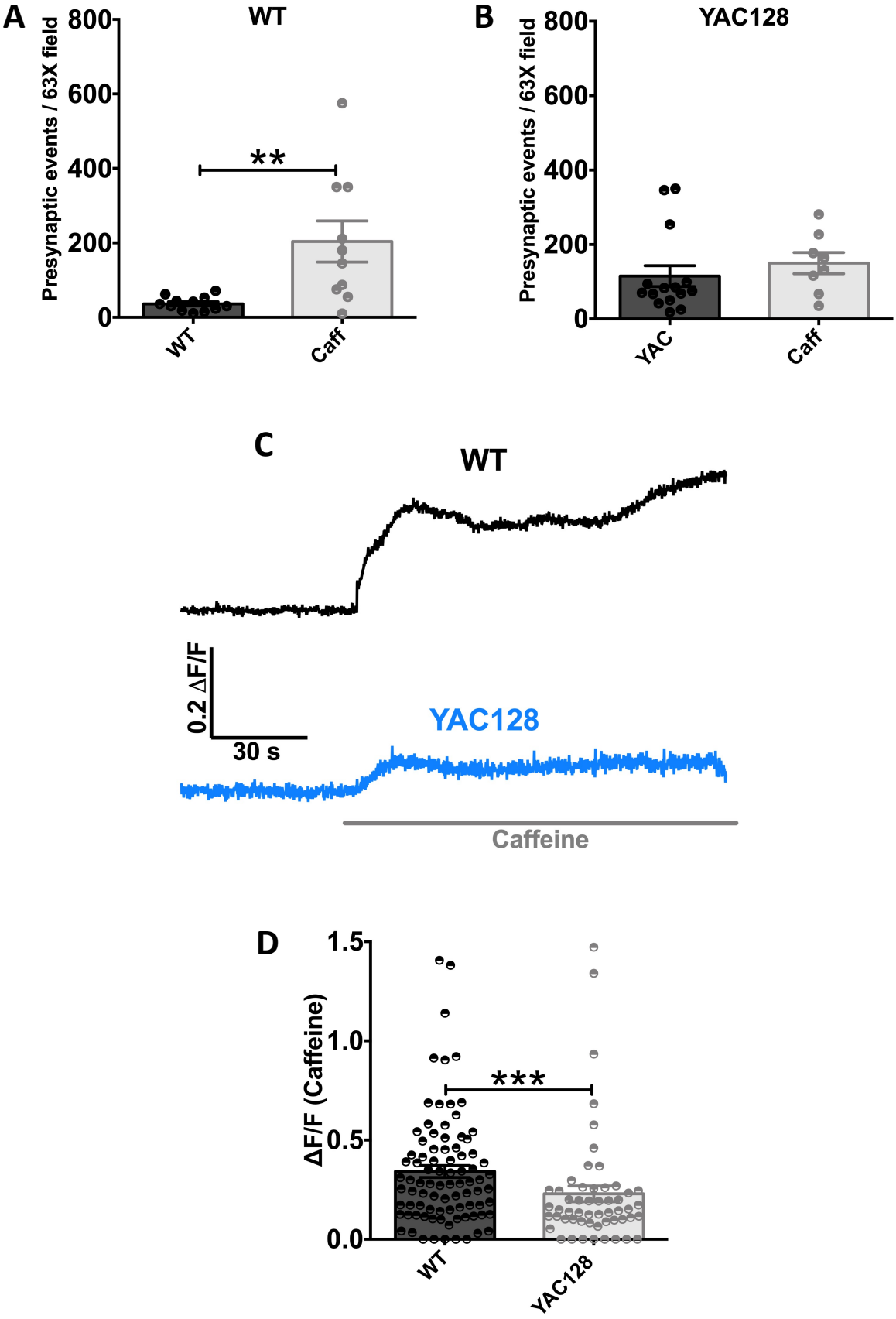
A
WT
Presynaptic events / 63X field
800
600
400
200
0
**
WT
Caff
B
YAC128
Presynaptic events / 63X field
800
600
400
200
0
YAC
Caff
C
WT
0.2 ΔF/F
30 s
YAC128
Caffeine
D
ΔF/F (Caffeine)
1.5
1.0
0.5
0.0
***
WT
YAC128

Figure 9:

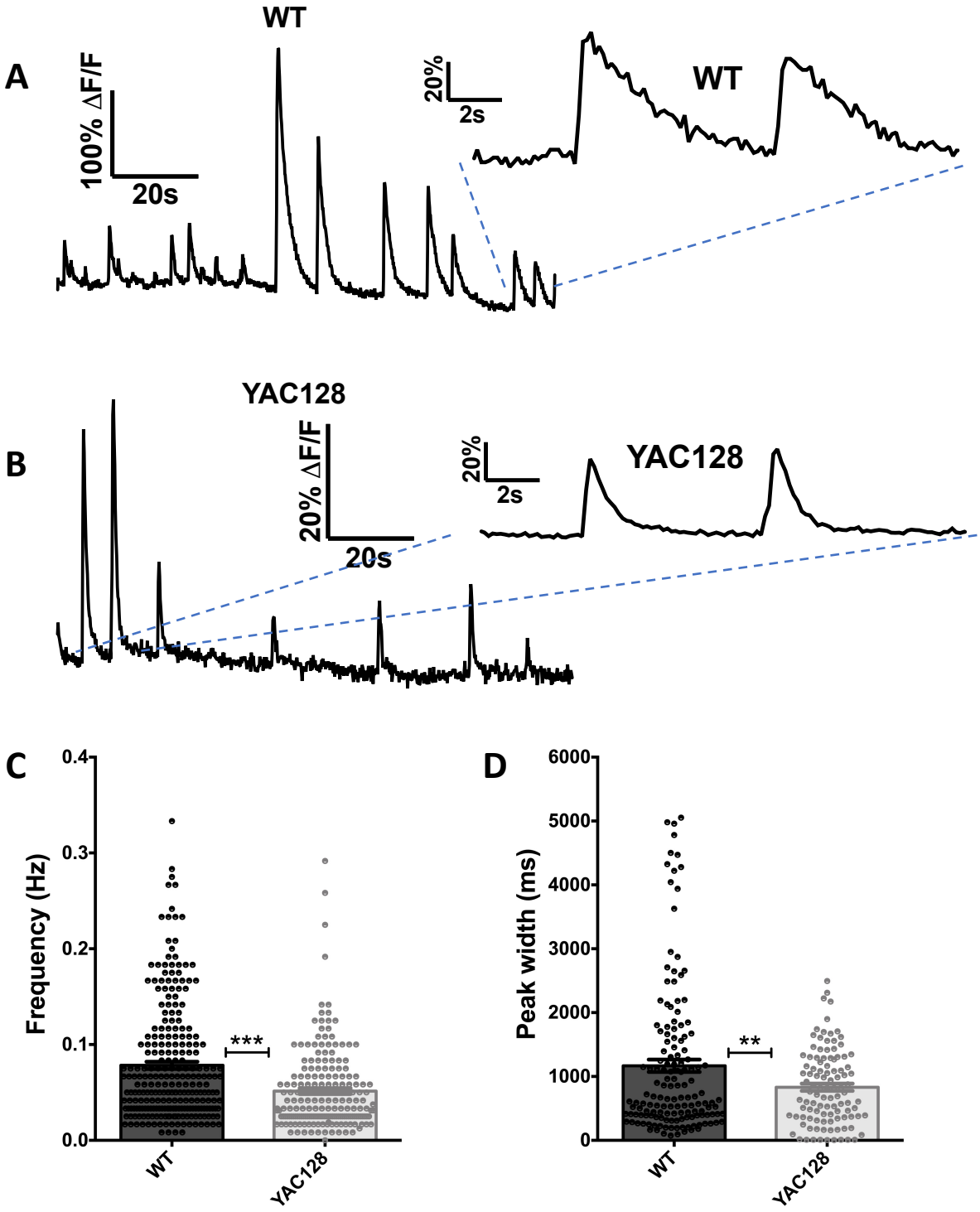
A
WT
100% ΔF/F
20s
20%
2s
WT
B
YAC128
20% ΔF/F
20s
20%
2s
YAC128
C
Frequency (Hz)
0.4
0.3
0.2
0.1
0.0
***
WT
YAC128
D
Peak width (ms)
6000
5000
4000
3000
2000
1000
0
**
WT
YAC128

Figure 10:

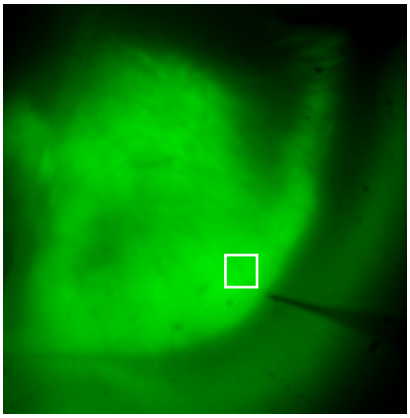

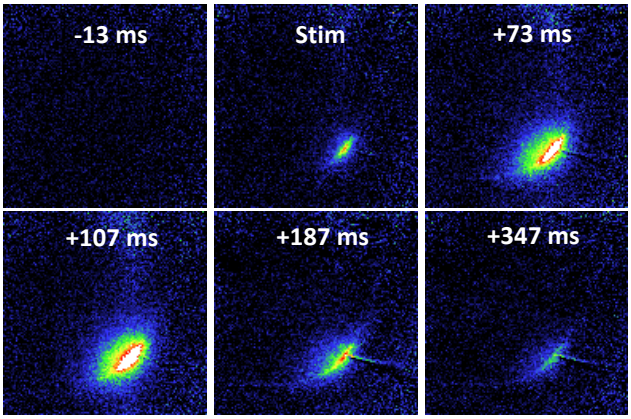
-13 ms
Stim
+73 ms
+107 ms
+187 ms
+347 ms

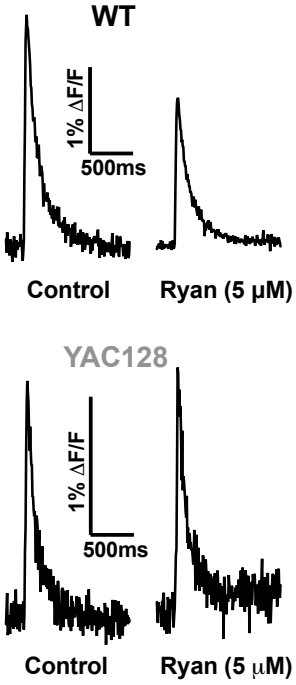
WT
1% ΔF/F
500ms
Control
Ryan (5 μM)
YAC128
1% ΔF/F
500ms
Control
Ryan (5 μM)

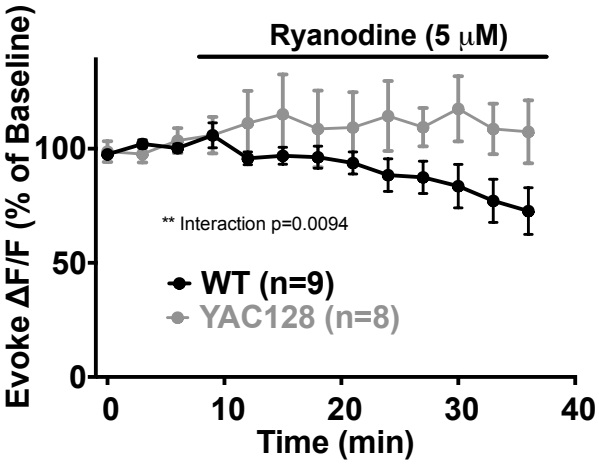
Ryanodine (5 μM)
Evoke ΔF/F (% of Baseline)
100
50
0
** Interaction p=0.0094
WT (n=9)
YAC128 (n=8)
0
10
20
30
40
Time (min)